Planetary Surfaces:

1. What define planetary surfaces geologically?

2. What controls the evolution of planetary surfaces?

3. How do surface-shaping processes scale across planetary bodies of different sizes, compositions, and physical states?

4. How do surface-shaping processes interact? What is the role of feedback?

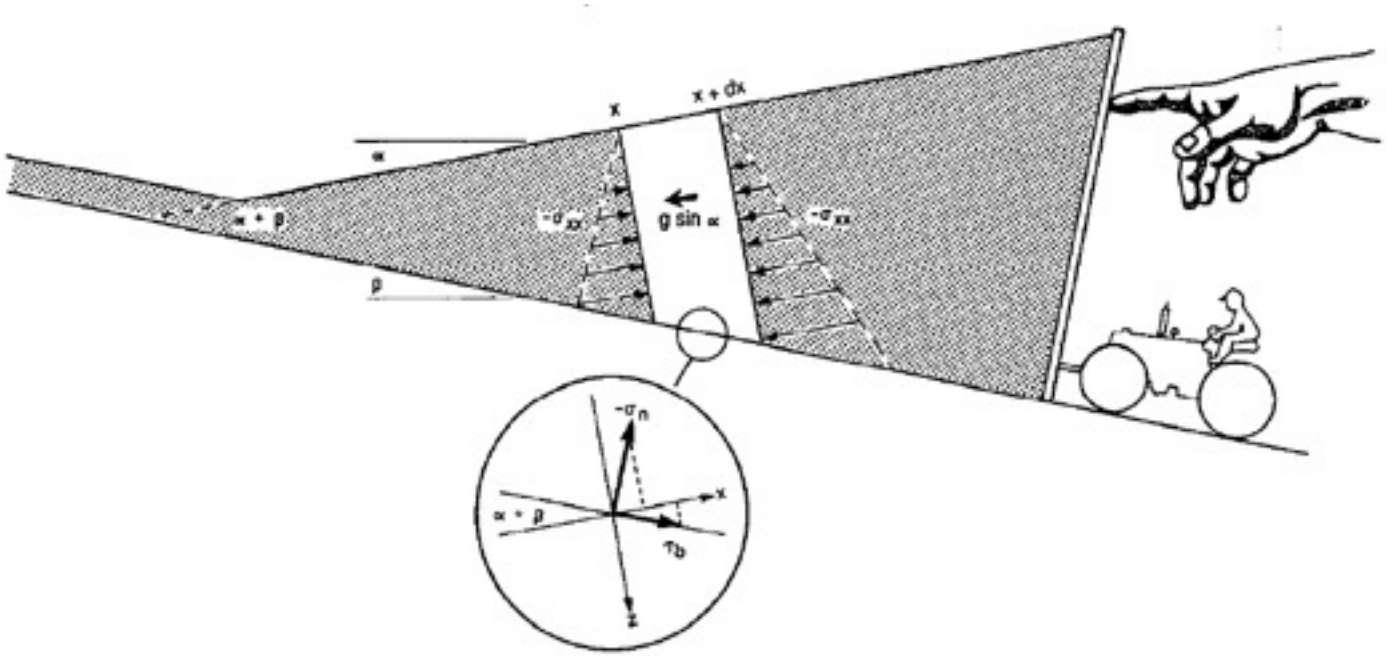

Figure 6 Schematic diagram illustrating the horizontal balance of forces on an element of a bulldozer wedge.

$$-\rho g H \sin\alpha - \sigma_n[\mu_b \cos(\alpha+\beta) + \sin(\alpha+\beta)] + \frac{d}{dx}\int_0^H \sigma_{xx}\, dz = 0.$$

Non-cohesive critical taper geometry is defined by:

$$\alpha + \beta \approx \left(\frac{1 - \sin \phi}{1 + \sin \phi} \right) (\beta + \mu_b)$$

Where α is surface slope, β is fault dip, μb coefficient of friction along the basal thrust, and ϕ is the angle of internal friction as defined in Coulomb fracture criterion when its cohesive strength is zero.

Brittle Fracture, a Quantitative Approach

Many people are interested in calculating when a material will break. The topic is of particular interest to earth scientists -- geomorphologists calculate the forces that lead to landslides, earthquake geologists evaluate the likelihood of a fault rupturing, and structural geologists want reconstruct paleostress fields from field observations of fractures and faults. The (Mohr-)Coulomb criteria is an empirically derived method for determining when a material will fail (break) under shear.

Coulomb fracture criterion states:

$$|\sigma^*_s| = c + \mu\sigma_n \text{ and } \mu = \tan\varphi \quad \text{(T\&M pg. 169)}$$

σ^*_s is the **critical shear stress**
(the shear stress that causes the material to fracture)
σ_n is the applied **normal stress**
φ is called the **angle of internal friction**
μ is called the **coefficient of internal friction**.
c is the **cohesion**
(resistance to fracture along a surface with no normal stress, or the "stickiness").

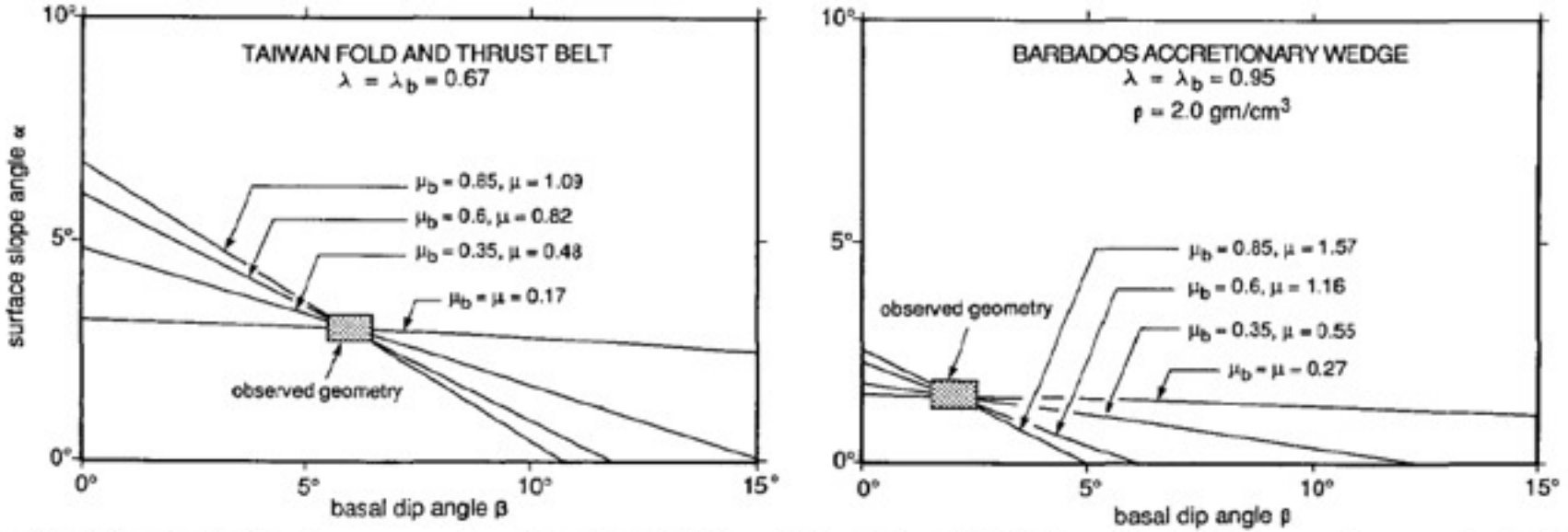

Figure 14 Theoretical surface slope α versus basal dip β for the Taiwan fold-and-thrust belt (*left*) and the Barbados accretionary wedge (*right*). Many possible combinations of μ_b and μ are consistent with the observed geometries and pore-fluid pressures.

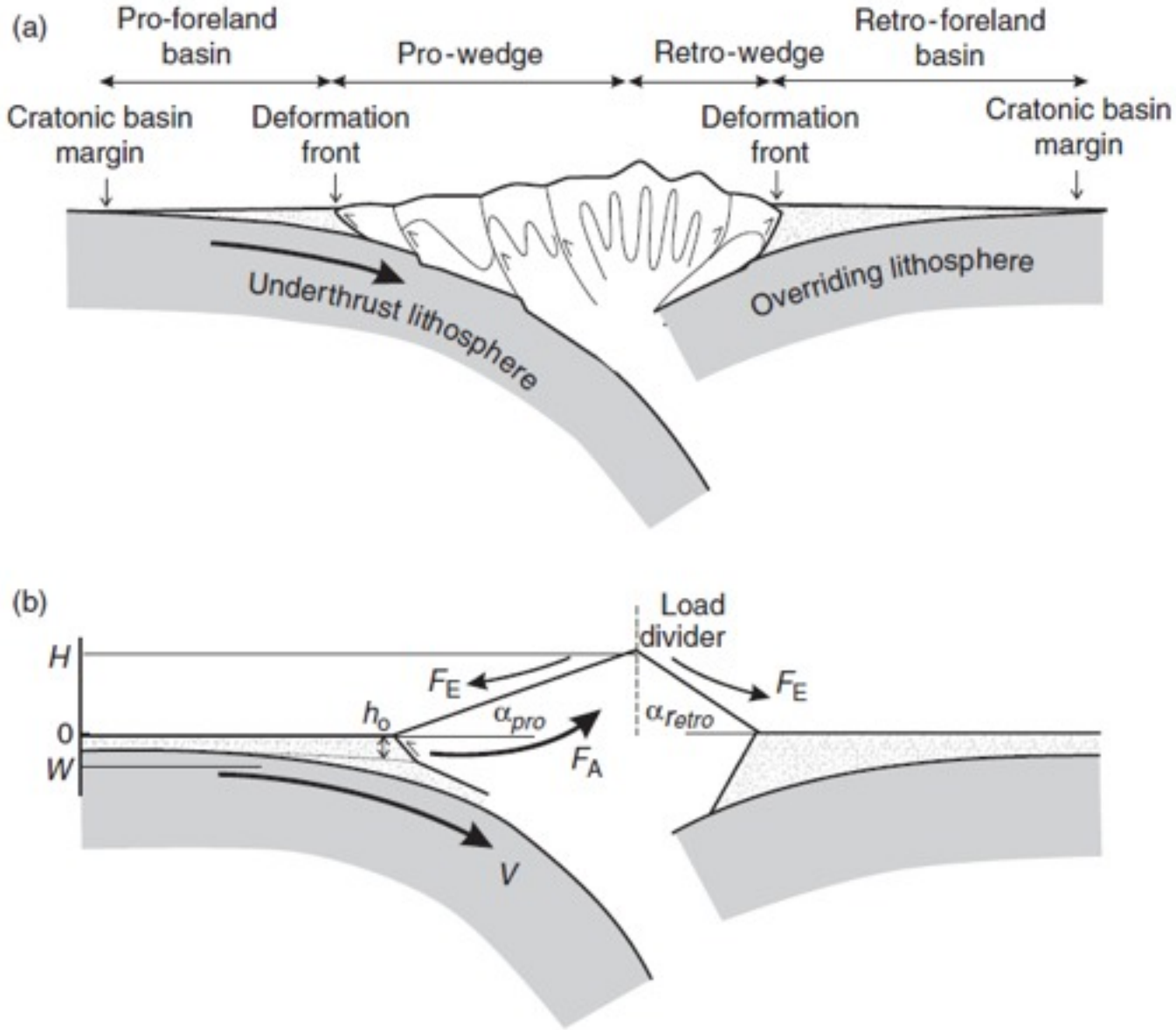

Naylor and Sinclair 2008

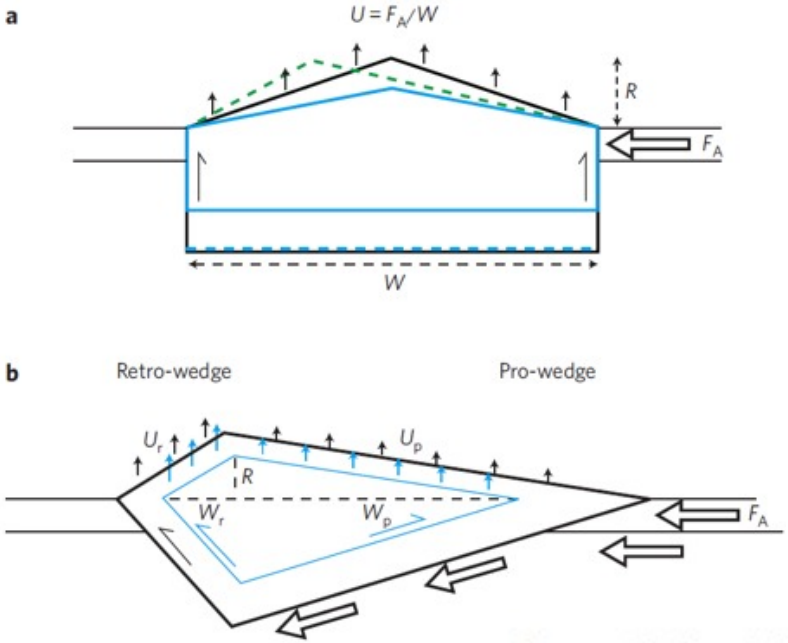

Whipple (2009)

Figure 3 | Analytical landscape-evolution models. Solid lines in both panels show topography and crustal root for low (black) and high (blue) erosional efficiency. **a**, Fixed-width orogen. The width of the orogen (W) and the accretionary flux (F_A) remain constant. Arrows show invariant steady-state near-surface rock uplift rates (U; assuming simple block-uplift). Climate-induced changes in erosional efficiency may lead to changes in relief (R) but do not affect the tectonics. Similarly, asymmetry in erosional efficiency leads to asymmetric topography (dashed green line), but no change in rock uplift rates. **b**, Critically tapered wedge. U_r and U_p are near-surface rock uplift rates (the length of the arrows are proportional to the uplift rates) on the retro- and pro- sides of the wedge, which have widths W_r and W_p, respectively. For constant accretionary flux, a climate-induced increase in erosional efficiency leads to a reduction in wedge size (blue lines) and a commensurate increase in the steady-state near-surface rock uplift rates (blue arrows).

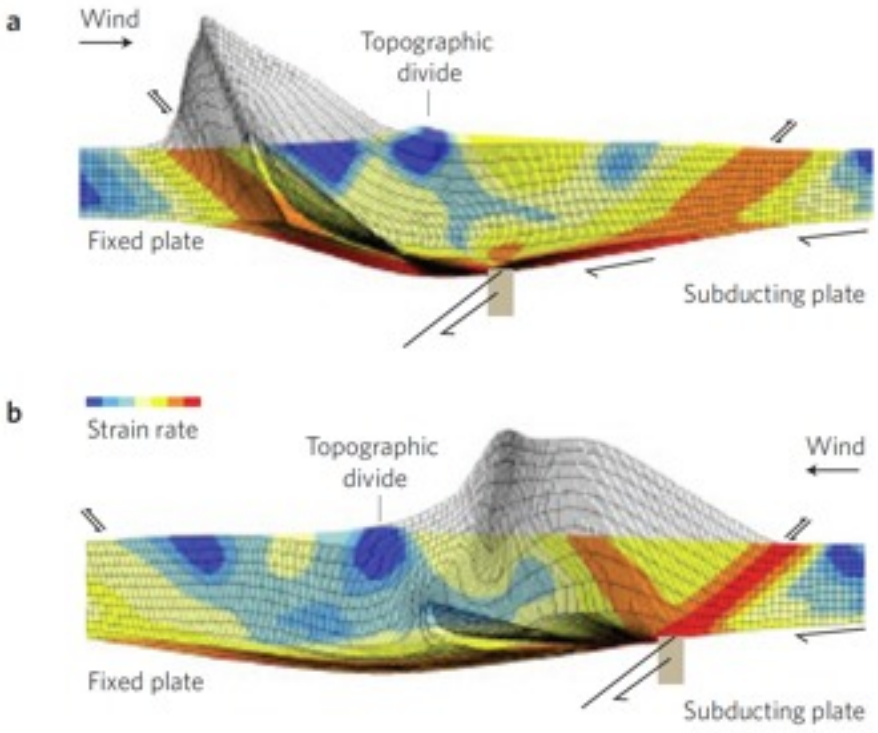

Figure 1 | Unidirectional moisture flux and mountain-belt evolution. **a**,**b**, Results of numerical models aimed at understanding the exhumational and structural response of mountain belts to unidirectional moisture flux. Tectonic convergence velocity and subduction direction in the models match conditions for the Southern Alps of New Zealand. In **a**, moisture-laden winds arrive from the west (left). Uplift and exhumation, indicated by the extension of the Lagrangian tracking mesh above the topographic surface (top of the coloured domain), is focused over an active thrust fault (orange band to the west, indicating high strain rate). In **b**, moisture-laden winds arrive from the east (right). Both uplift and exhumation are focused east of the drainage divide. The western thrust fault (the same as in **a**) is nearly inactive. **c**, The observed topography and pattern of total uplift and exhumation (difference between topography and total uplift) in the Southern Alps closely match the numerical experiment shown in **a**. Panels **a** and **b** used with permission from ref. 8 (© 1999 AGU); panel **c** reprinted with permission from ref. 7 (© 1990 GSA).

Willett 1999

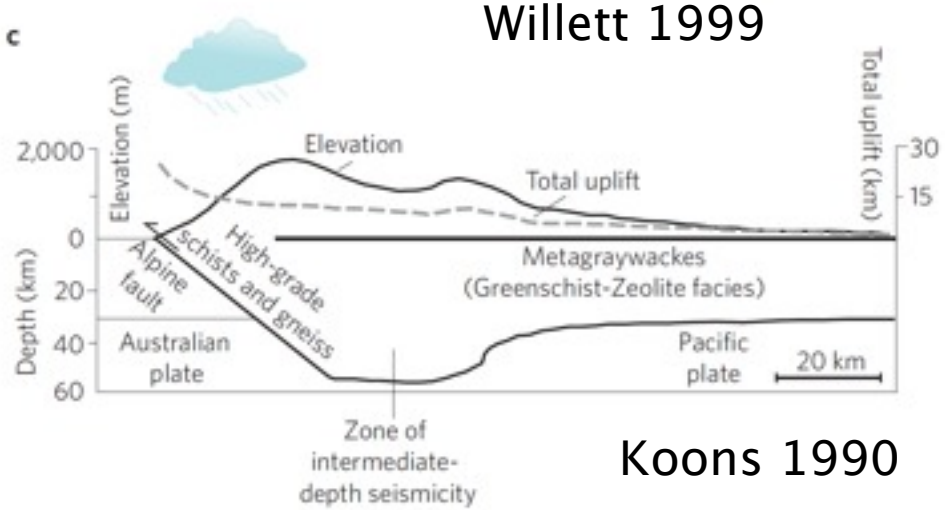

Koons 1990

Case study in the New Zealand Alps.

Case study in the Himalaya

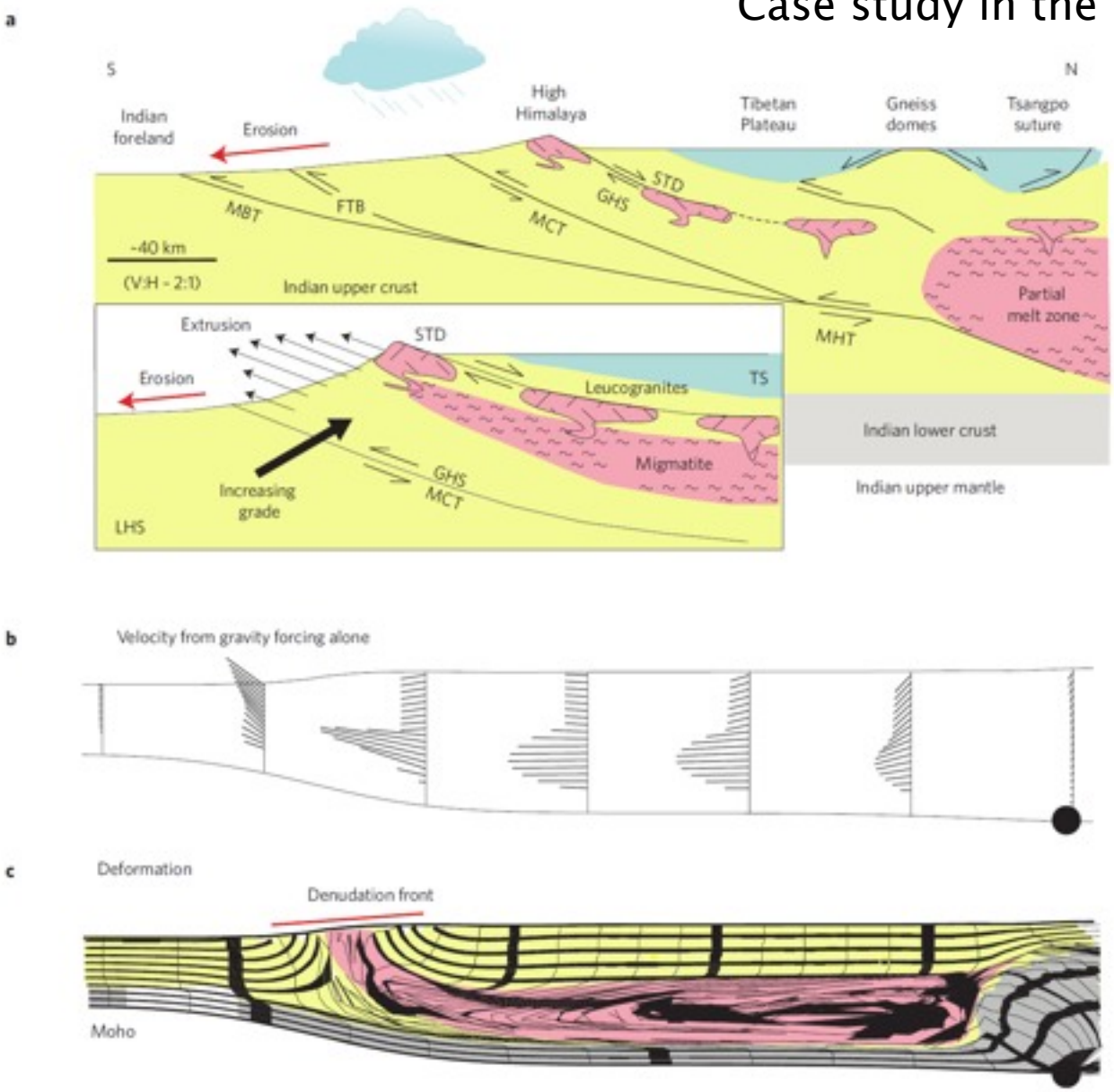

Beaumont et al. (2001)

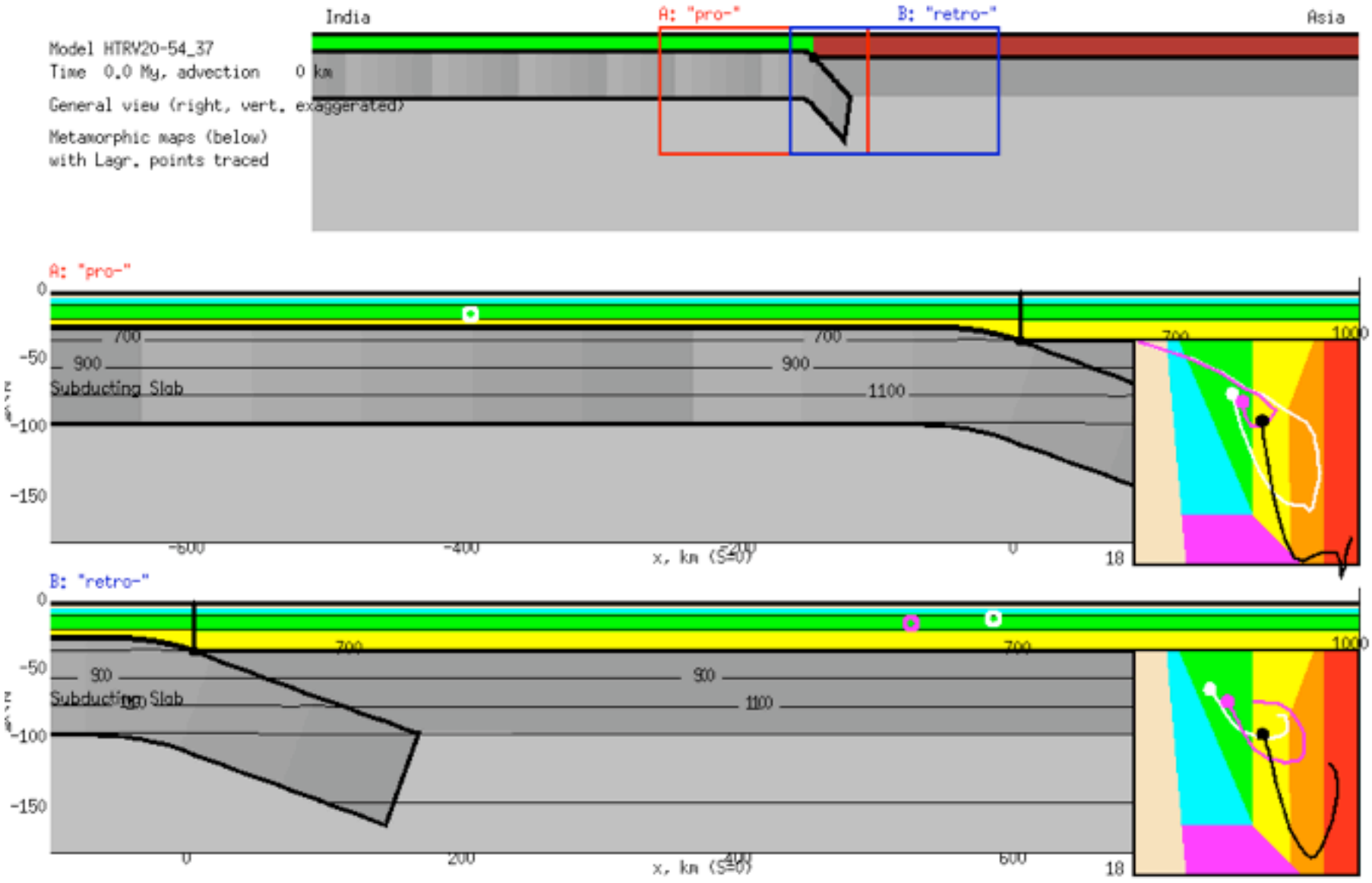
India
A: "pro-"
B: "retro-"
Asia
Model HTRV20-54_37
Time 0.0 My, advection
0 km
General view (right, vert. exaggerated)
Metamorphic maps (below)
with Lagr. points traced
A: "pro-"
0
-50
-100
-150
700
900
1100
Subducting Slab
-600
-400
-200
0
x, km (S=0)
18
B: "retro-"
0
-50
-100
-150
700
900
1100
Subducting Slab
0
200
400
600
x, km (S=0)
18

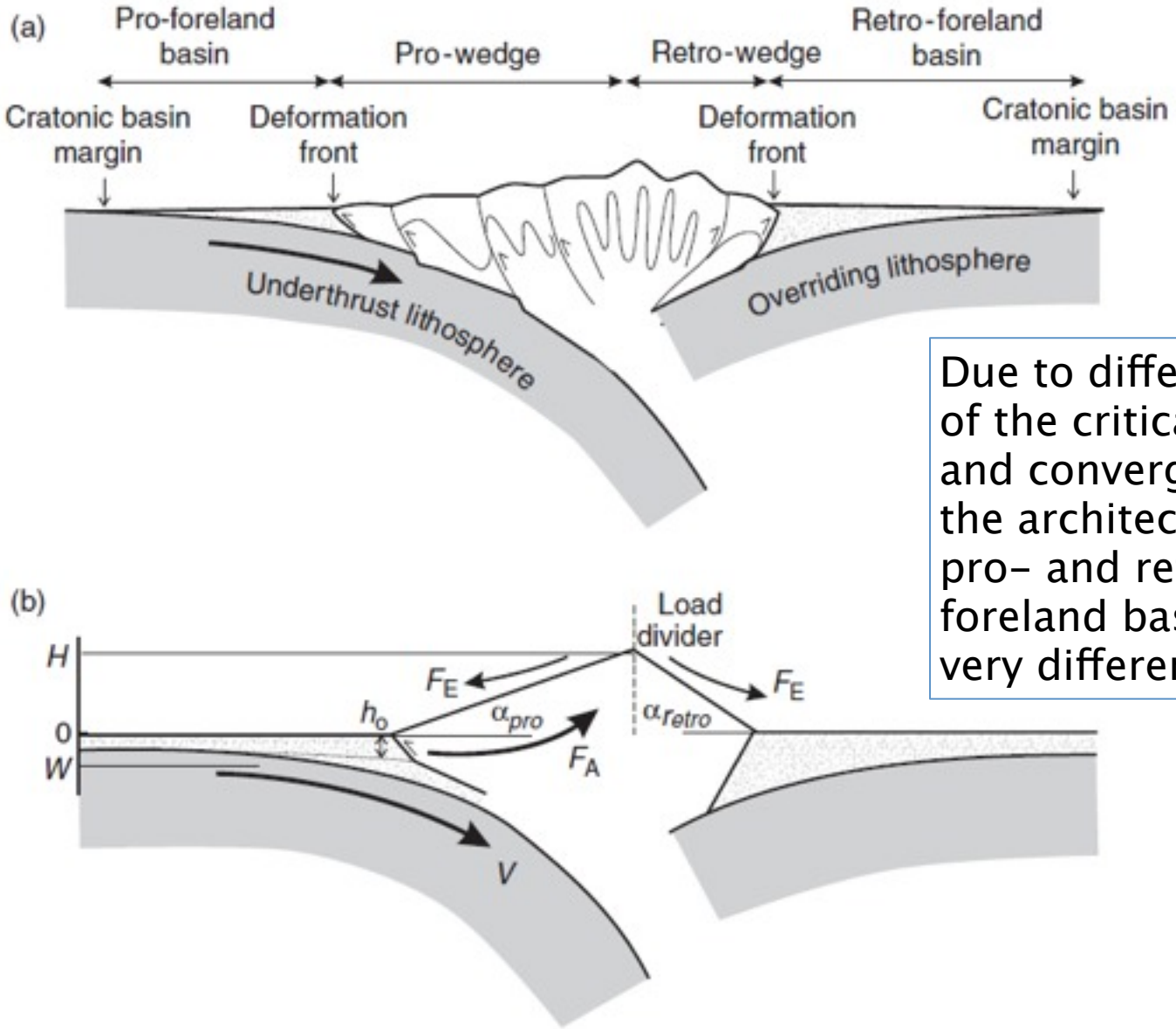

Due to different shapes of the critical wedges and convergence rates, the architectures of the pro- and retro-wedge foreland basins can be very different.

Naylor and Sinclair 2008

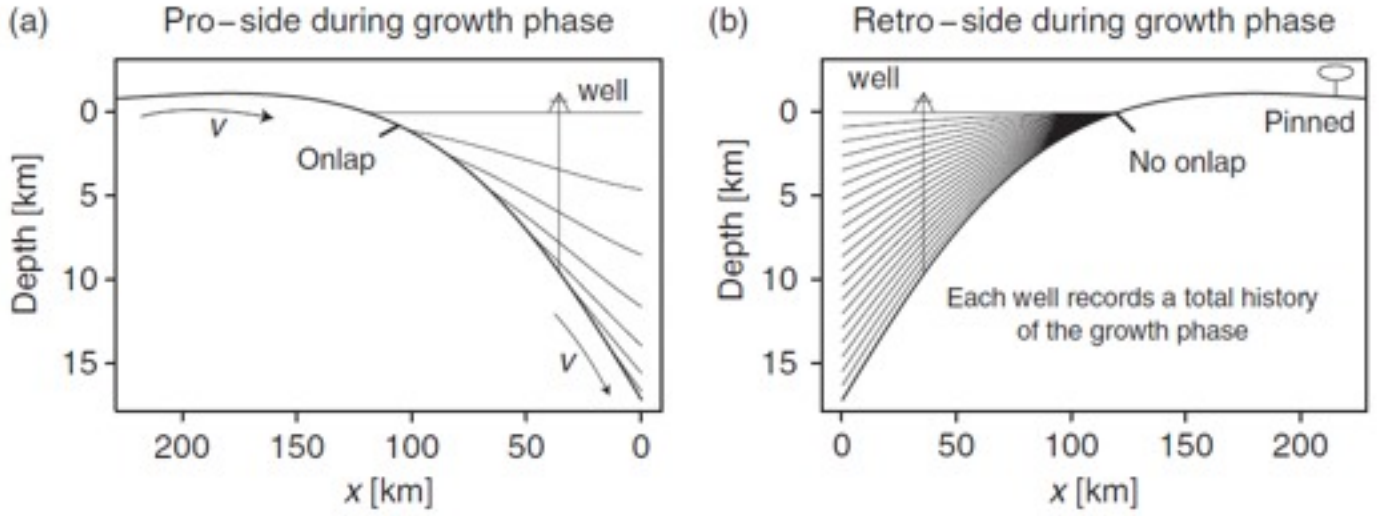

Fig. 3. Stratigraphic profiles for a pro- and retro-foreland basin modelled using an endload, applied at $x = 0$, during (a) and (b) the growth phase and (c) and (d) the steady-state phase. The stratigraphic horizons are spaced at 3.55 Myr intervals. The total duration for each run is 71 Myr. A well drilled in the retro-side basin records the entire growth phase. A well drilled in the pro-side only records a stratigraphic record related to the recent advection of the basin.

Example of feedback interactions between faulting and surface processes

(Ice loading leading to acceleration of faulting creating rift dams, followed diversion of major rivers, creating river anticlines across the Himalaya).

Feedback processes between normal faulting and surface processes (erosion of the rift shoulder and sedimentation in the hanging wall)

Earth and Planetary Science Letters 284 (2009) 570–582

Contents lists available at ScienceDirect

Earth and Planetary Science Letters

journal homepage: www.elsevier.com/locate/epsl

Slip acceleration on normal faults due to erosion and sedimentation — Results from a new three-dimensional numerical model coupling tectonics and landscape evolution

Georgios Maniatis [a,*], Daniel Kurfeß [b], Andrea Hampel [a], Oliver Heidbach [c]

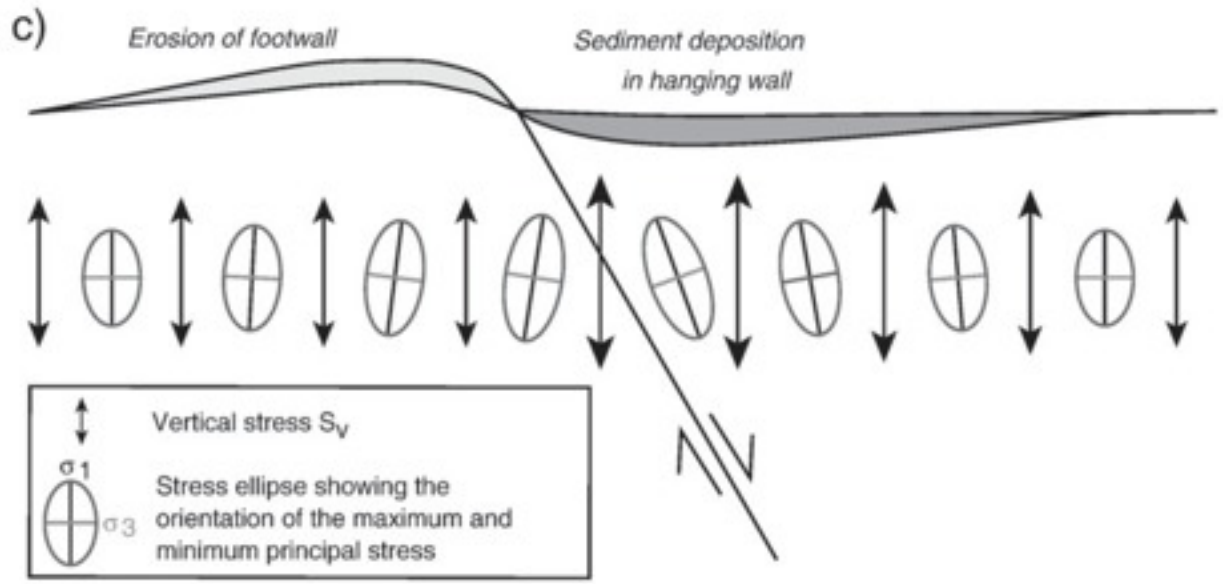
c)
Erosion of footwall
Sediment deposition
in hanging wall
Vertical stress S_v
σ1
σ3
Stress ellipse showing the orientation of the maximum and minimum principal stress

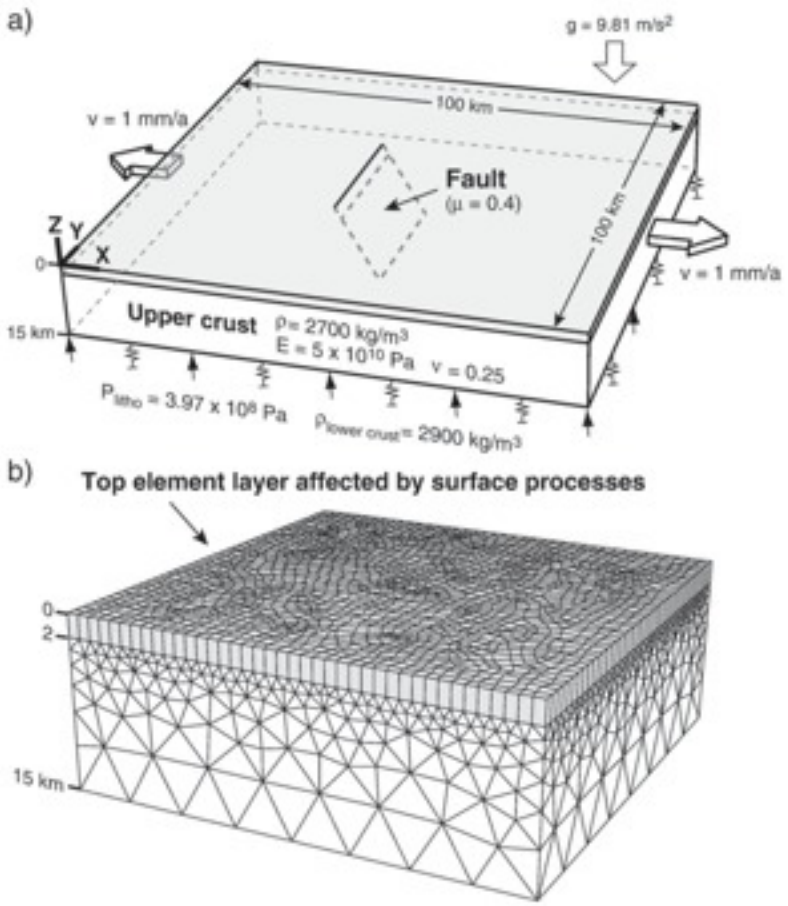
a)
g = 9.81 m/s²
v = 1 mm/a
100 km
Fault
(μ = 0.4)
100 km
Z Y
X
0
v = 1 mm/a
Upper crust
ρ = 2700 kg/m³
E = 5 x 10¹⁰ Pa
ν = 0.25
15 km
P_litho = 3.97 x 10⁸ Pa
ρ_lower crust = 2900 kg/m³
b)
Top element layer affected by surface processes
0
2
15 km

Role of Diffusion in accelerating fault slip

Erosion follows diffusion law

$$\frac{\partial h}{\partial t} = k_D \nabla^2 h$$

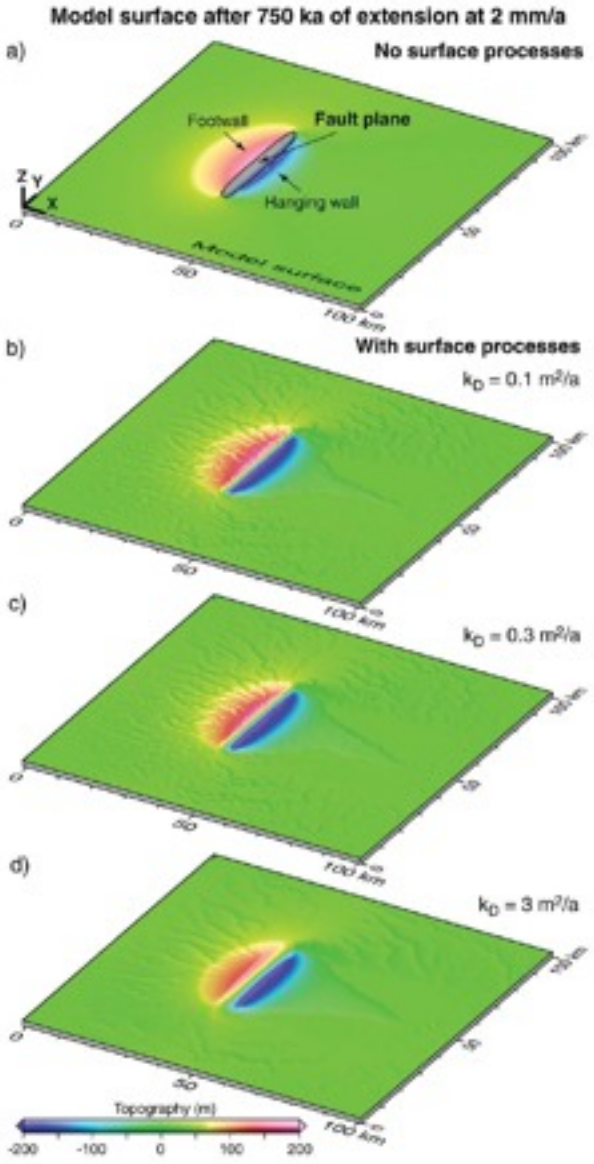

Effect of fault dip in the feedback processes

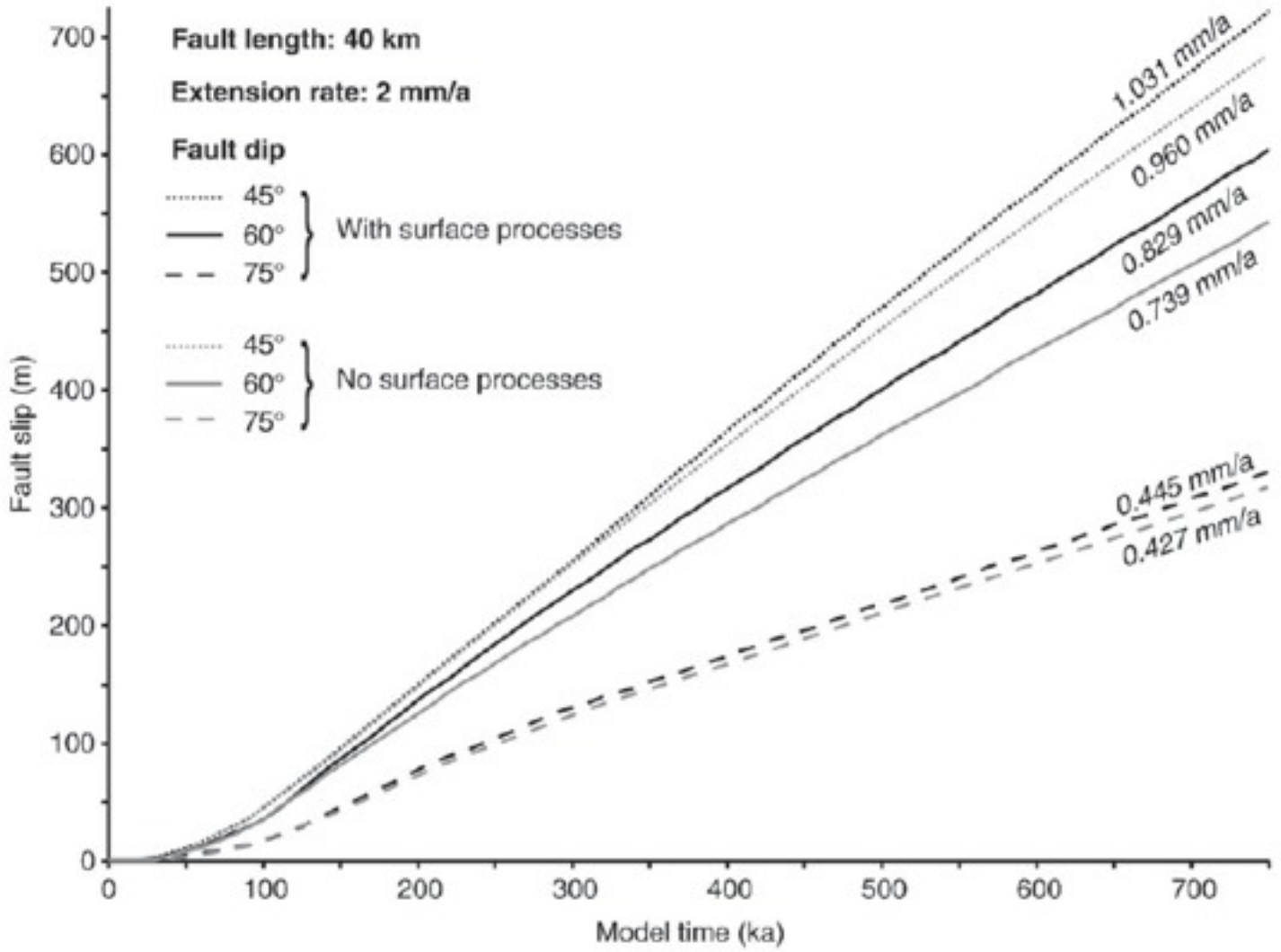

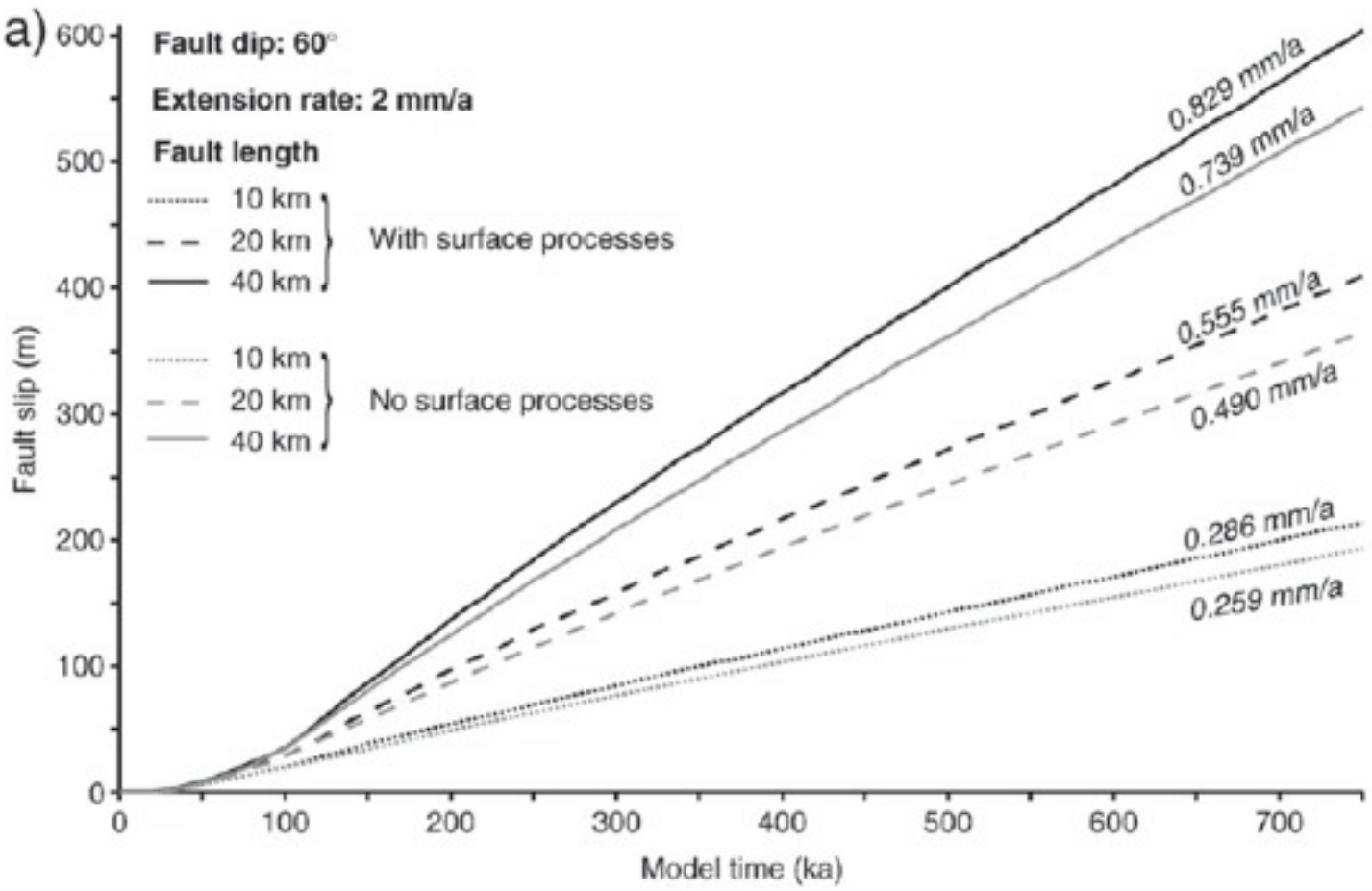

Maniatis et al. (2009, EPSL)

Feedback Processes between Faulting and Surface Processes for a group of faults

JOURNAL OF GEOPHYSICAL RESEARCH, VOL. 114, B08406, doi:10.1029/2008JB006113, 2009

Three-dimensional numerical modeling of slip rate variations on normal and thrust fault arrays during ice cap growth and melting

Andrea Hampel,[1] Ralf Hetzel,[2] Georgios Maniatis,[1] and Tobias Karow[1]

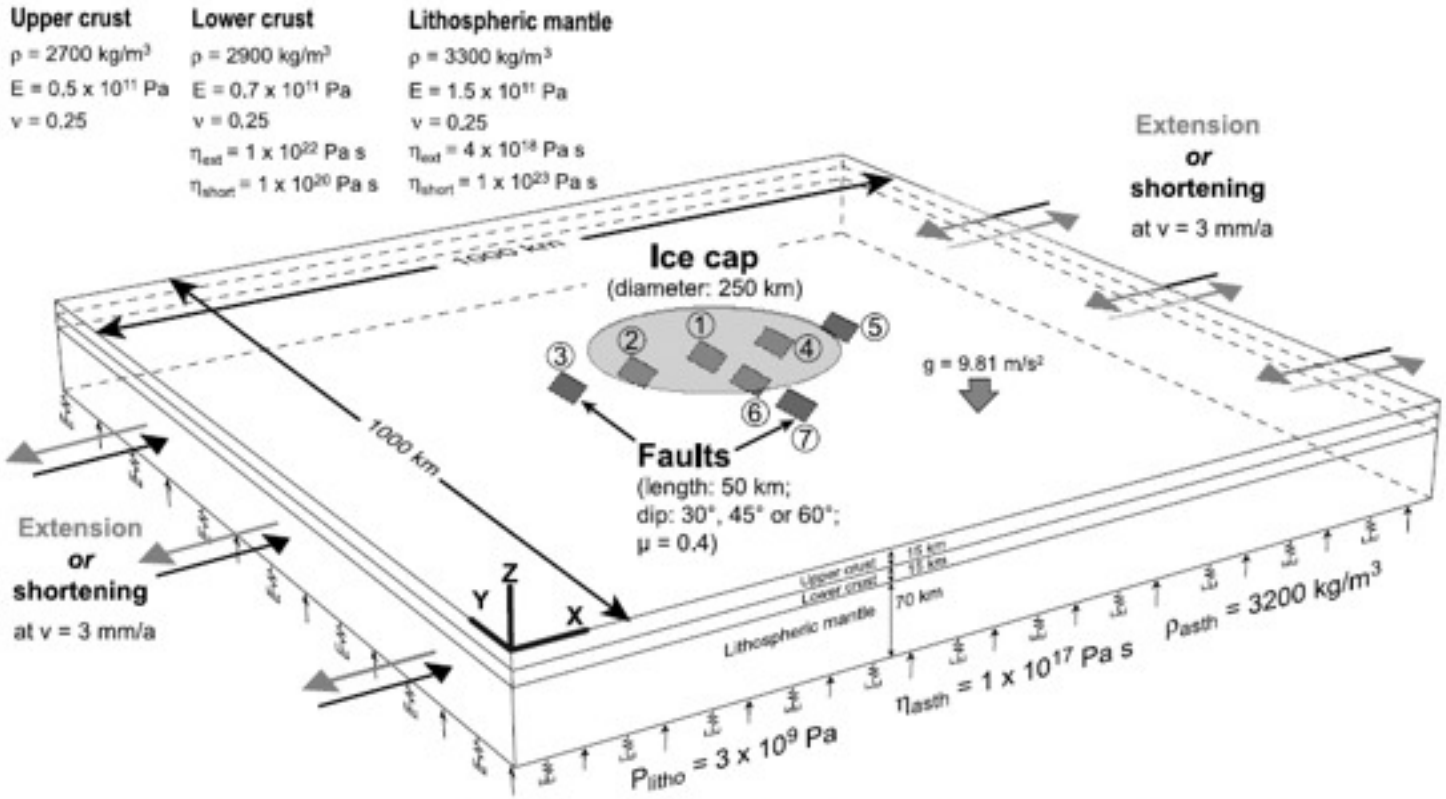

Figure 1. Perspective view of the finite element model. An array of seven faults is embedded in the upper crust; their dip is varied between 30°, 45°, and 60°. The grey circle marks the area where the pressure equivalent to a 1-km-thick ice cap was applied. The rheological parameters are density (ρ), Young's modulus (E), Poisson's ratio (ν), and viscosity (η). Gravity is included the model as a body force (acceleration due to gravity g = 9.81 m/s^2). Isostatic effects are implemented by adding a lithostatic pressure (P_{litho}), an elastic foundation, and linear dashpot elements to the bottom of the model. The properties of the elastic foundation and the dashpots represent an asthenosphere with a density of ρ = 3200 kg/m^3 and a viscosity of $\eta = 1 \times 10^{17}$ Pa s, respectively. In two different sets of experiments, the lithosphere is either extended or shortened at a total velocity of v = 6 mm/a on both sides in the yz plane. The bottom of the model is free to move in the vertical and the horizontal directions; model sides in the xz plane are fixed in the y direction. Slip initiation on the faults is controlled by a Coulomb failure criterion (μ is coefficient of friction).

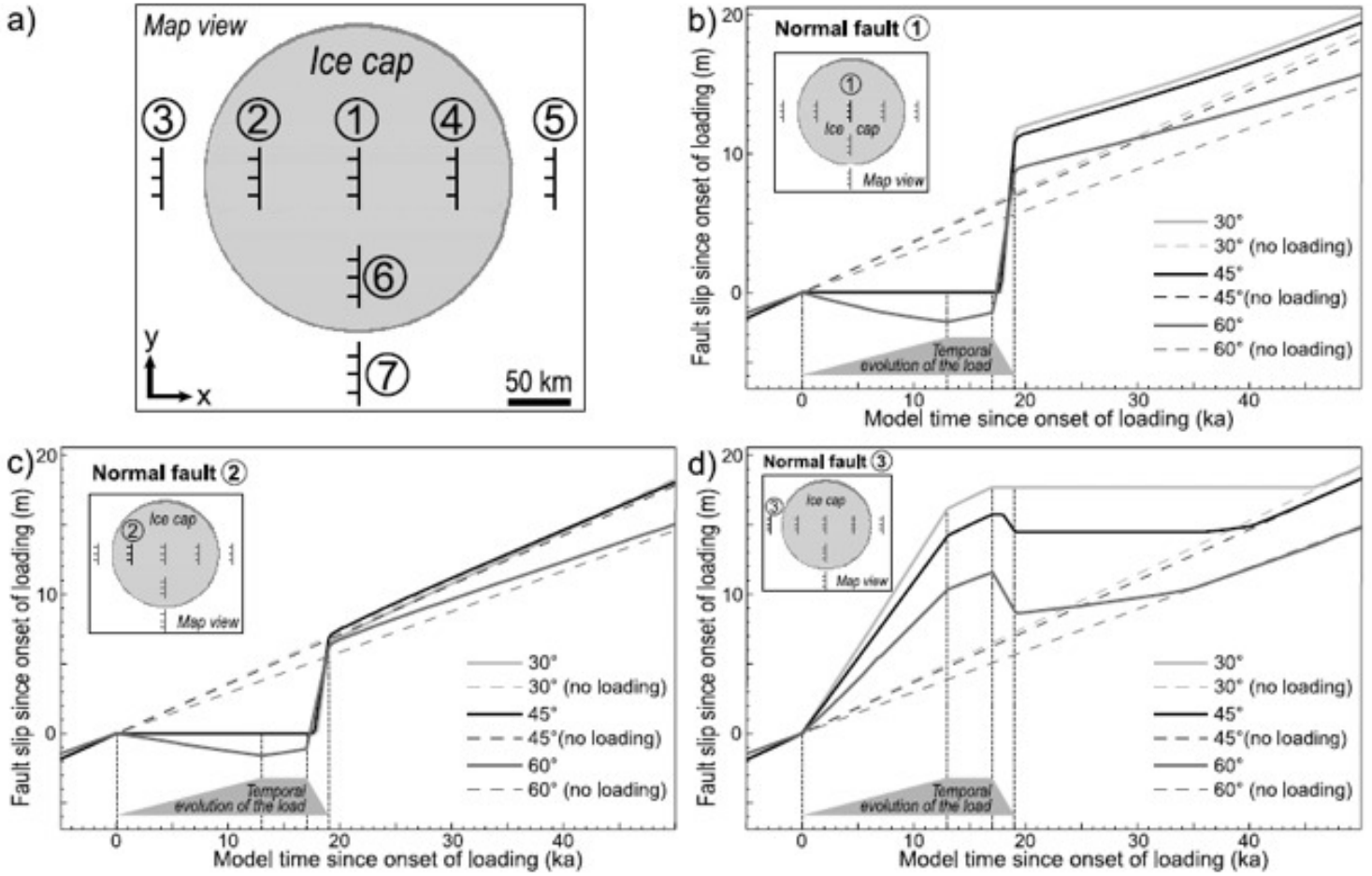

Figure 2. Results of the normal fault experiments carried out with fault dips of 30°, 45°, and 60°. (a) Map view of the model surface showing the number and the position of the faults relative to the ice cap. (b–h) Slip evolution at the center of faults 1–7 on the surface, respectively. Solid lines are slip curves extracted from experiments with loading and subsequent unloading. Dashed lines show the slip evolution of experiments without loading. The temporal evolution of the load is indicated by the gray polygon beneath the slip curves. Bars on the hanging walls of the faults mark the downthrown block.

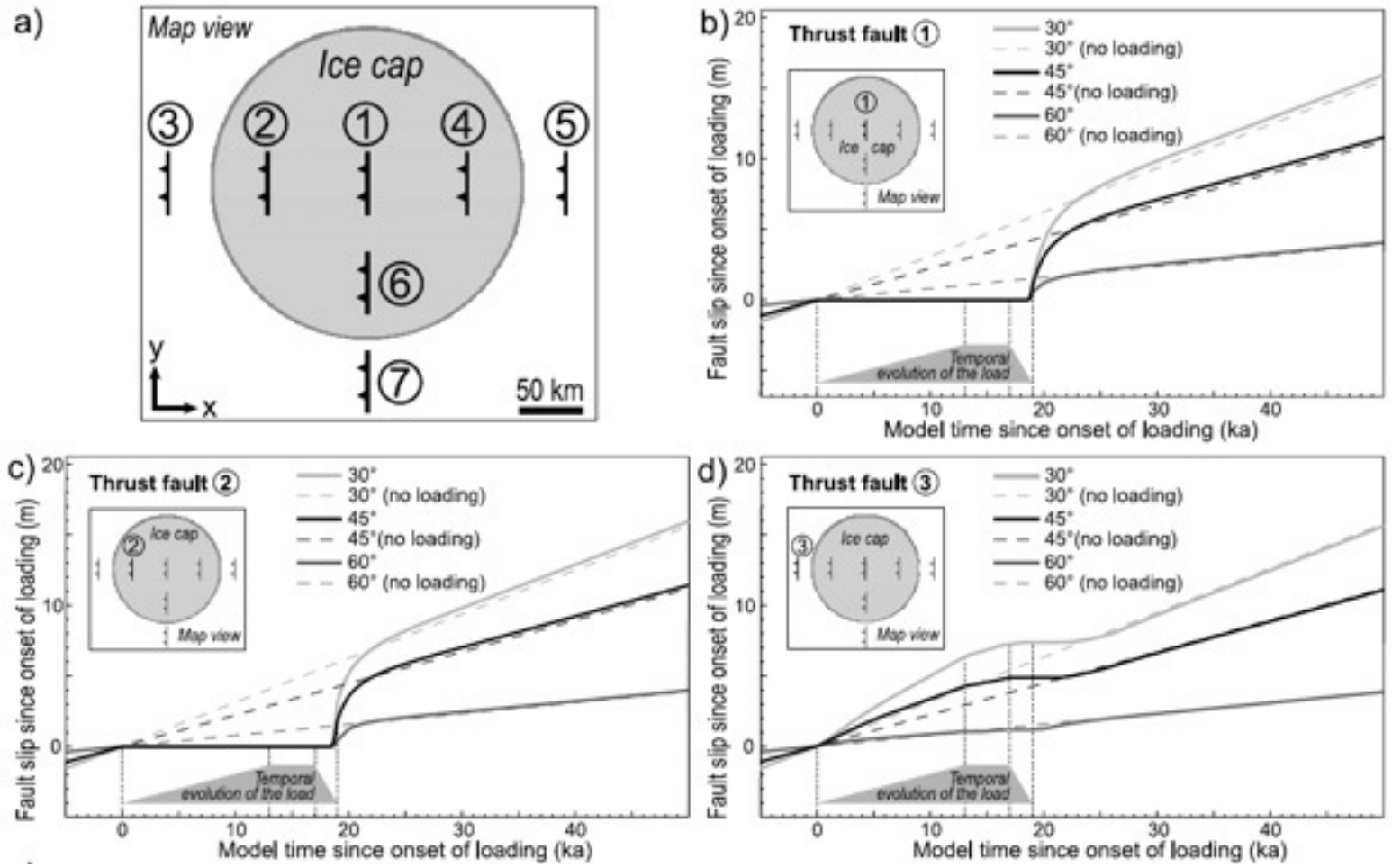

Figure 3. Results of the thrust fault experiments carried out with fault dips of 30°, 45°, and 60°. (a) Map view of the model surface showing the number and the position of the faults relative to the ice cap. (b–h) Slip evolution on the center of faults 1–7 on the surface, respectively. Solid lines are slip curves extracted from experiments with loading and subsequent unloading. Dashed lines show the slip evolution of experiments without loading. The temporal evolution of the load is indicated by the gray polygon below the slip curves. Triangles on the hanging walls of the faults mark the upthrown block.

Example of feedback processes in alternating the drainage system across the and its landscape

Two concepts:

1. **Rift damming**

2. **River anticlines**

If uplift is too fast, it can defeat the river flowing across the rift

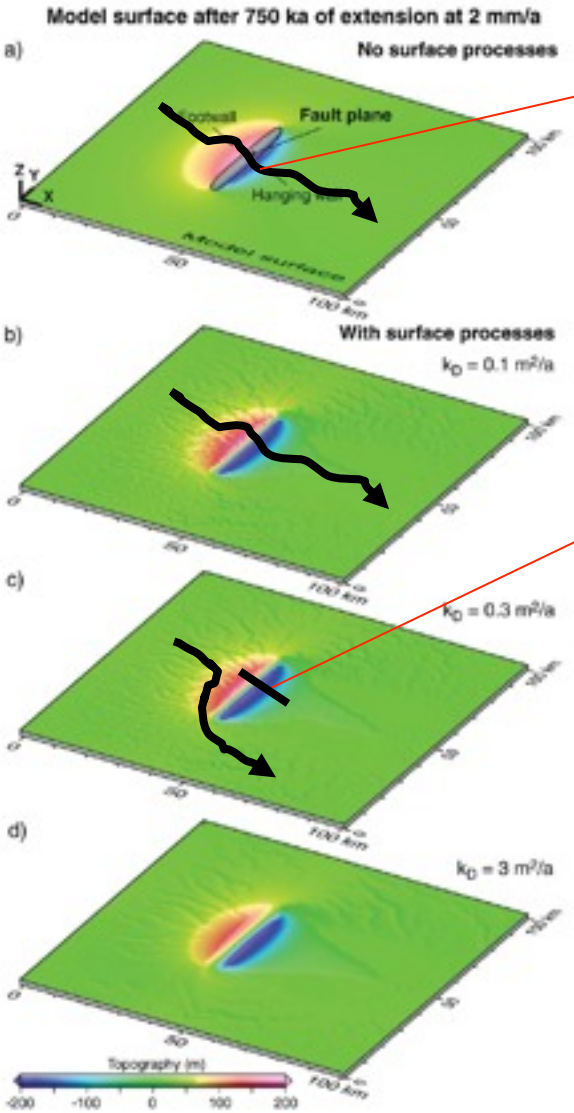

Water gap = gorge

Wind gas

River anticline

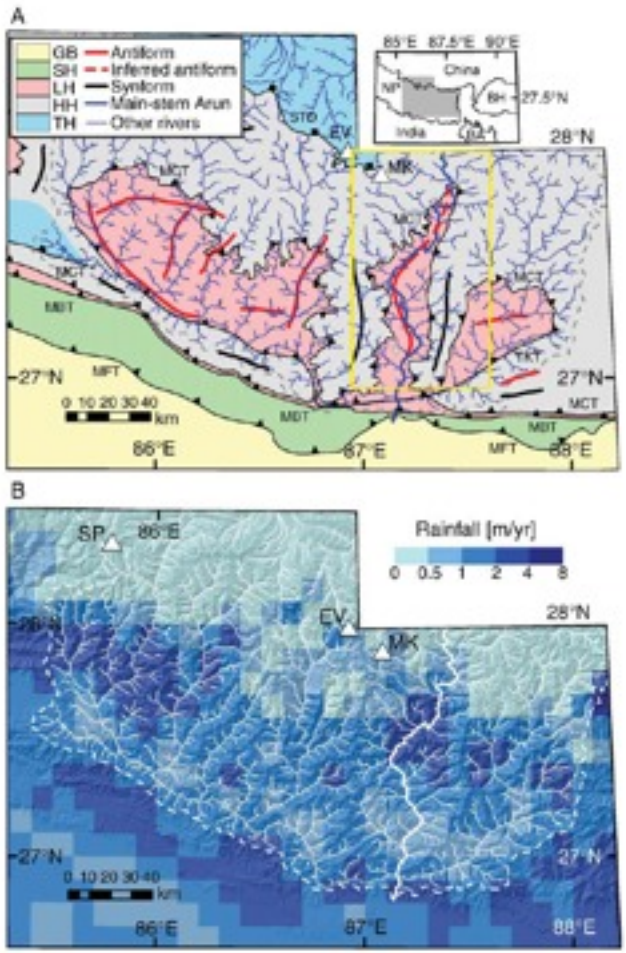

Fig. 1. (A) Geologic map of eastern Nepal (after Schelling, 1992), and (B) precipitation map draped on shaded DEM of the area. Triangles show locations of major peaks (EV = Everest; MK = Makalu; SP = Shisha Pangma). Inset shows location of study area (NP = Nepal; BH = Bhutan; BA = Bangladesh). Stratigraphic abbreviations are as follows: GB = Ganges Basin, SH = Sub-Himalaya; LH = Lesser Himalaya; HH = High Himalaya; TH = Tibetan Himalaya. Structural abbreviations are: MFT = main frontal thrust; MBT = main boundary thrust; MCT = main central detachment; STD = South Tibetan detachment; TKT = Tamar Kola Thrust.

Major Cenozoic tectonics events in the Himalaya:

1. Shortening of Northern Himalayas at 50-20 Ma.
2. Shortening of Southern Himalaya started at 20 Ma (MCT) and has continued to the present (MBT and MFT).
3. Initiation of north-trending rifts at about 10-8 Ma.

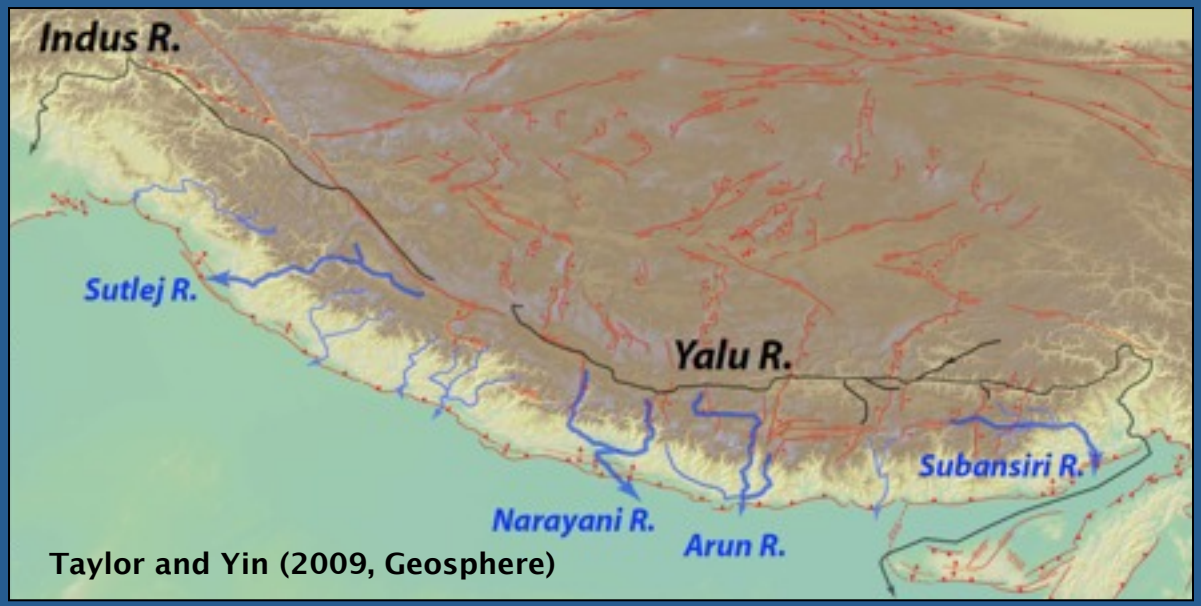

Taylor and Yin (2009, Geosphere)

Dominant structures in the Himalaya: Orogen-parallel thrusts and orogen-perpendicular rifts

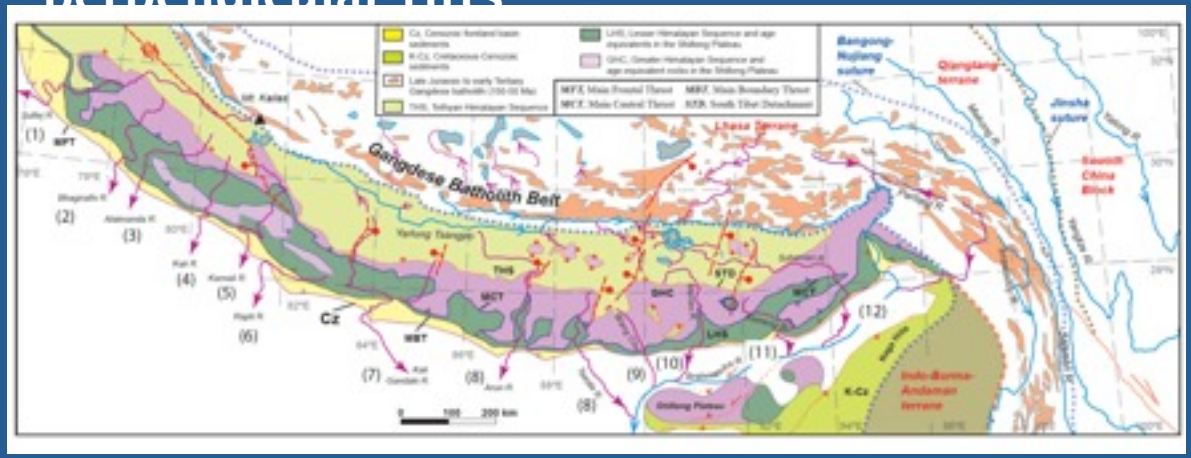

Quaternary Himalayan glacial history

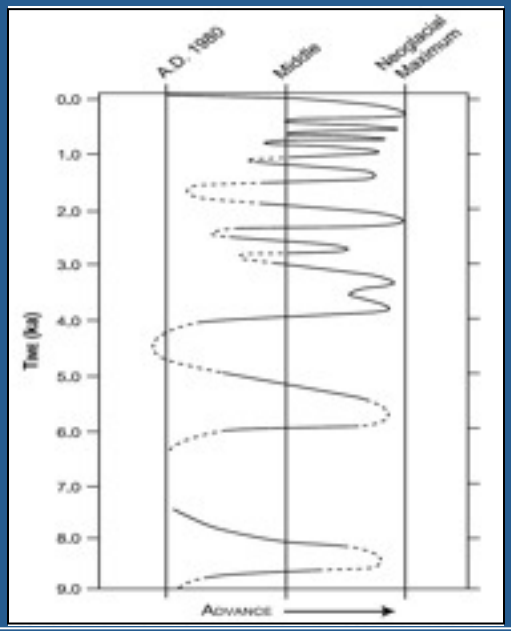

Owen (2009, Quat Sci. Rev)

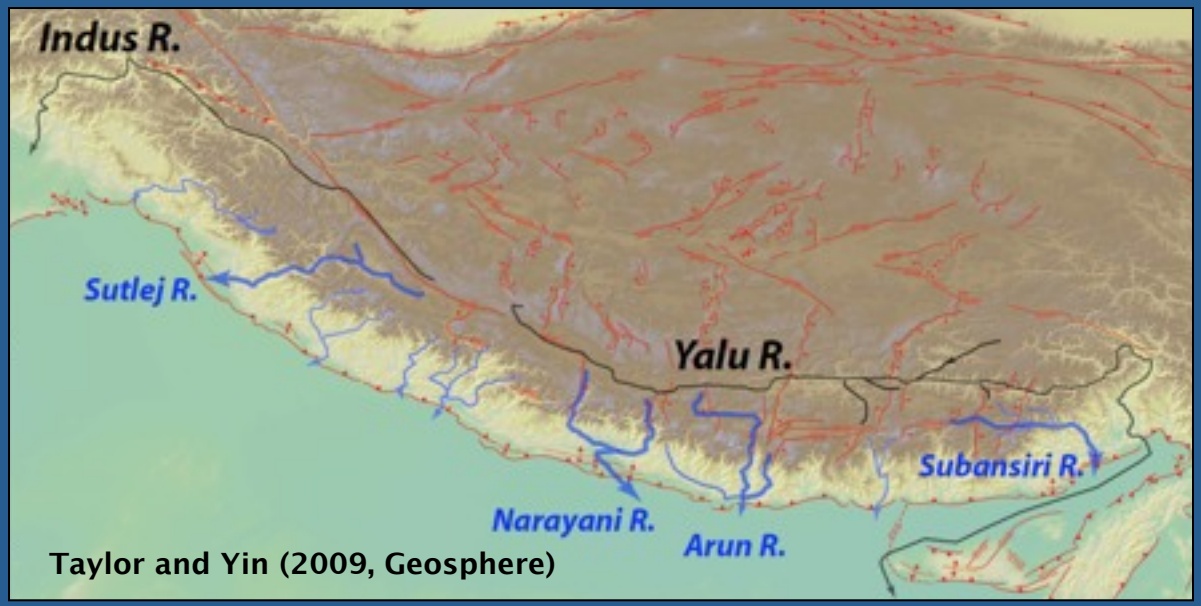

Taylor and Yin (2009, Geosphere)

Cenozoic seawater Sr and paleo-atmospheric CO2

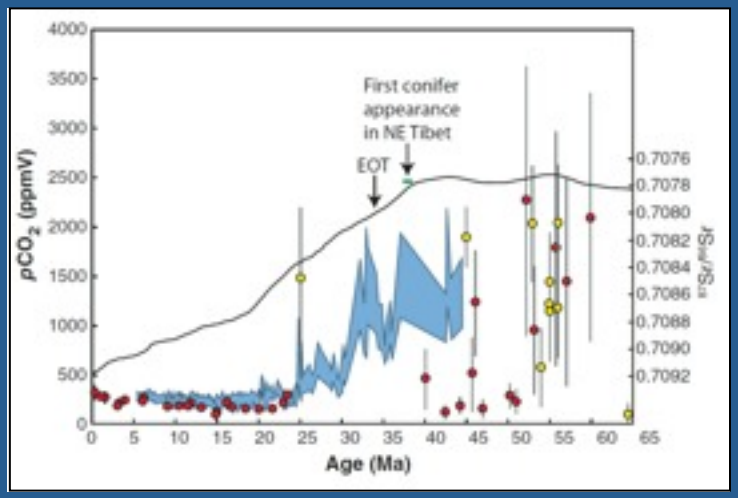

Garzione (2008, Geology)

Himalayan tectonic events have been interacting with global and local climate changes (e.g., repeated glacial advances in the Quaternary and gradual global cooling since the Eocene-Oligocene boundary).

A river course is a faithful expression of topography and thus its history provides important information on past morphologic evolution. The Yarlung Tsangpo separates the Tibetan plateau from the Himalaya. The two have very different rock types: the former is composed of an arc while the latter composed of continental margin sequence and its basement.

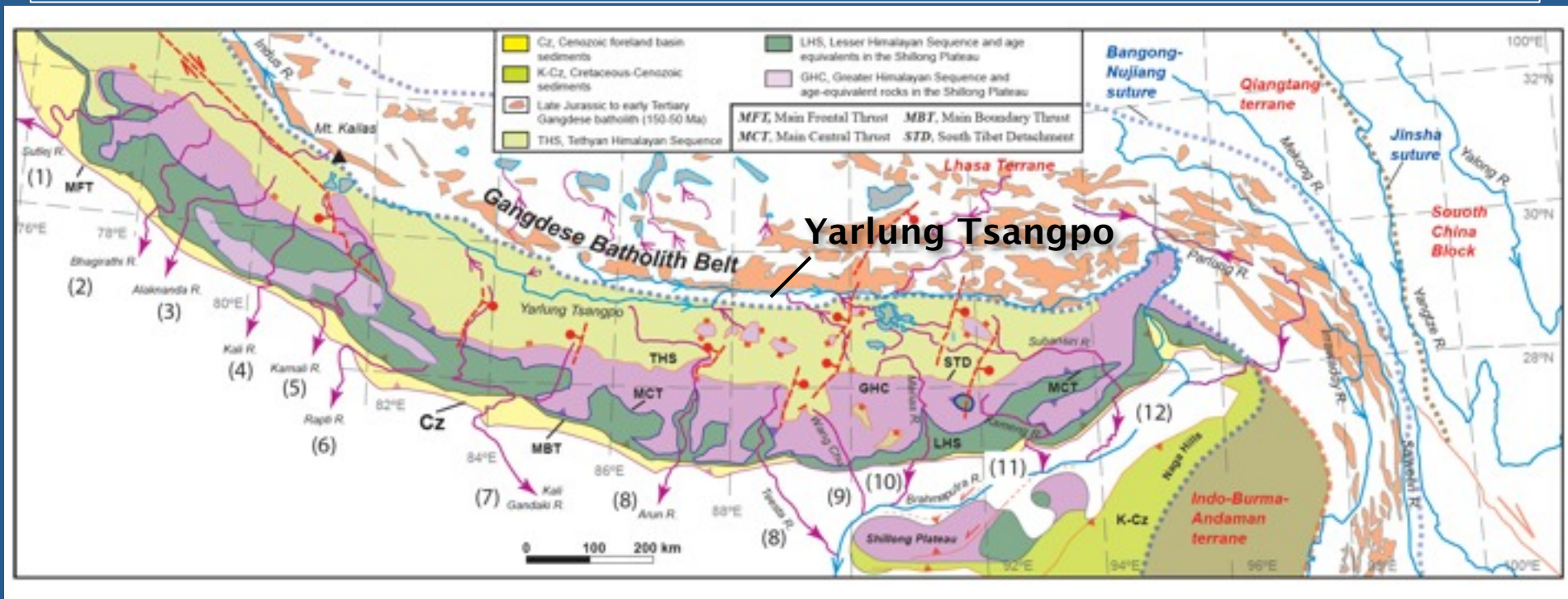

Flow reversal of the Yarlung Tsangpo (Yalu River) was long speculated by Burrard and Hayden (1907), but no records of such events were found and no causes were proposed.

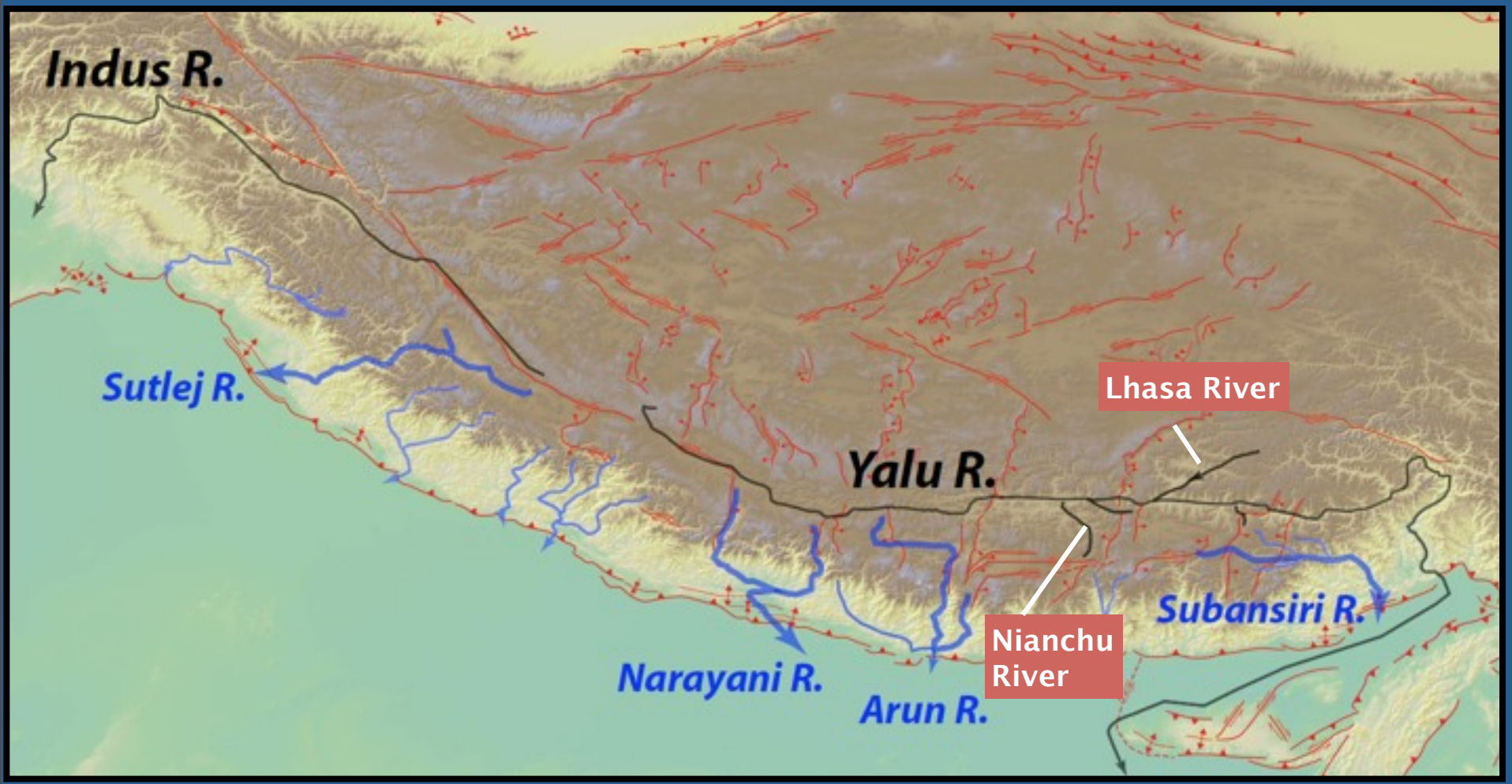

Observations:

1. Presence of Gangdese-batholith detrital zircons in the eastern Himalayan foreland basin sediments (Cina et al., 2009 EPSL).
2. Rifts have caused damming and ponding of large modern lakes in southern Tibet

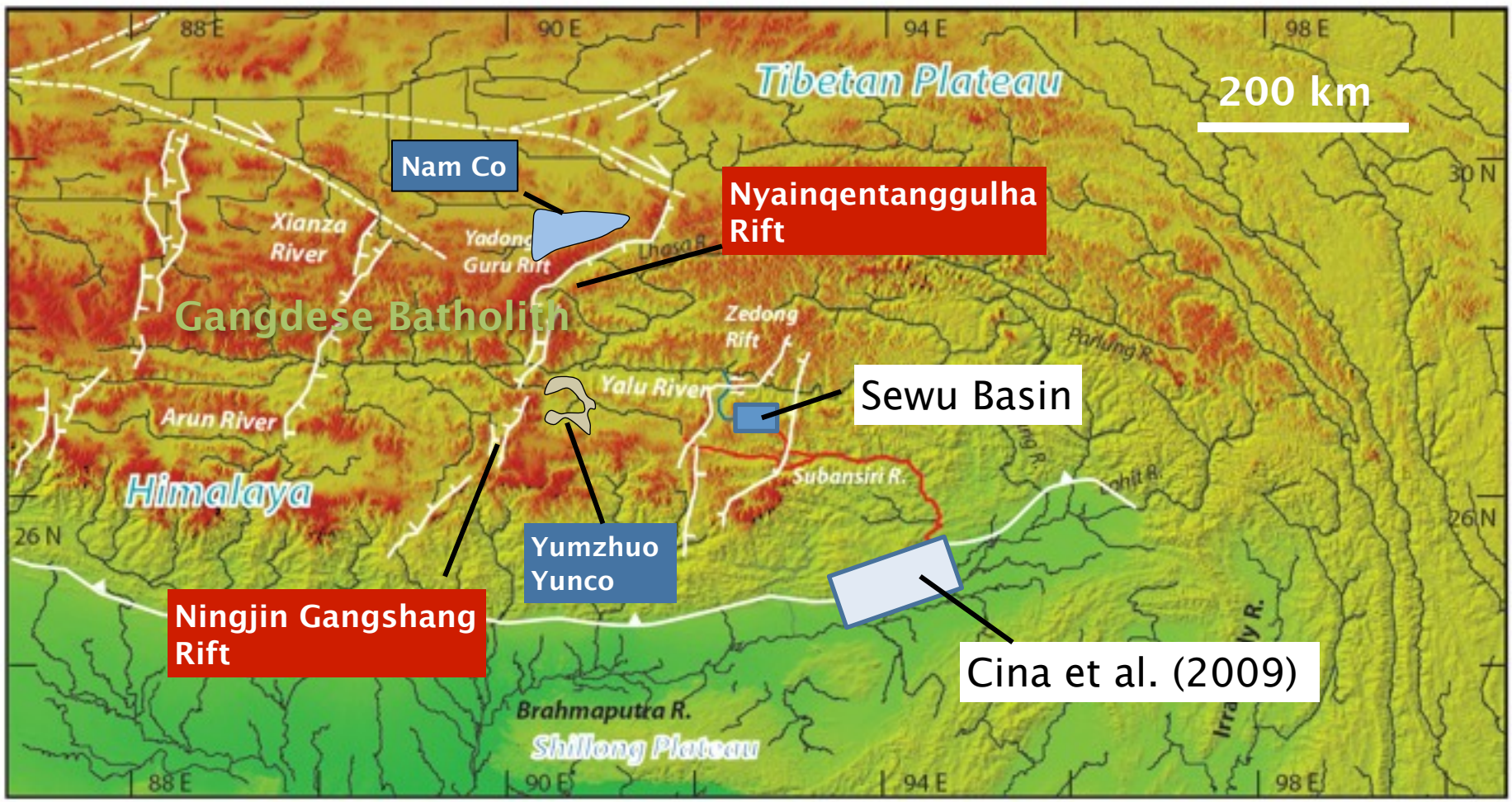

Presence of Gangdese-batholith detrital zircons in the eastern Himalayan foreland basin sediments (Cina et al., 2009 EPSL).

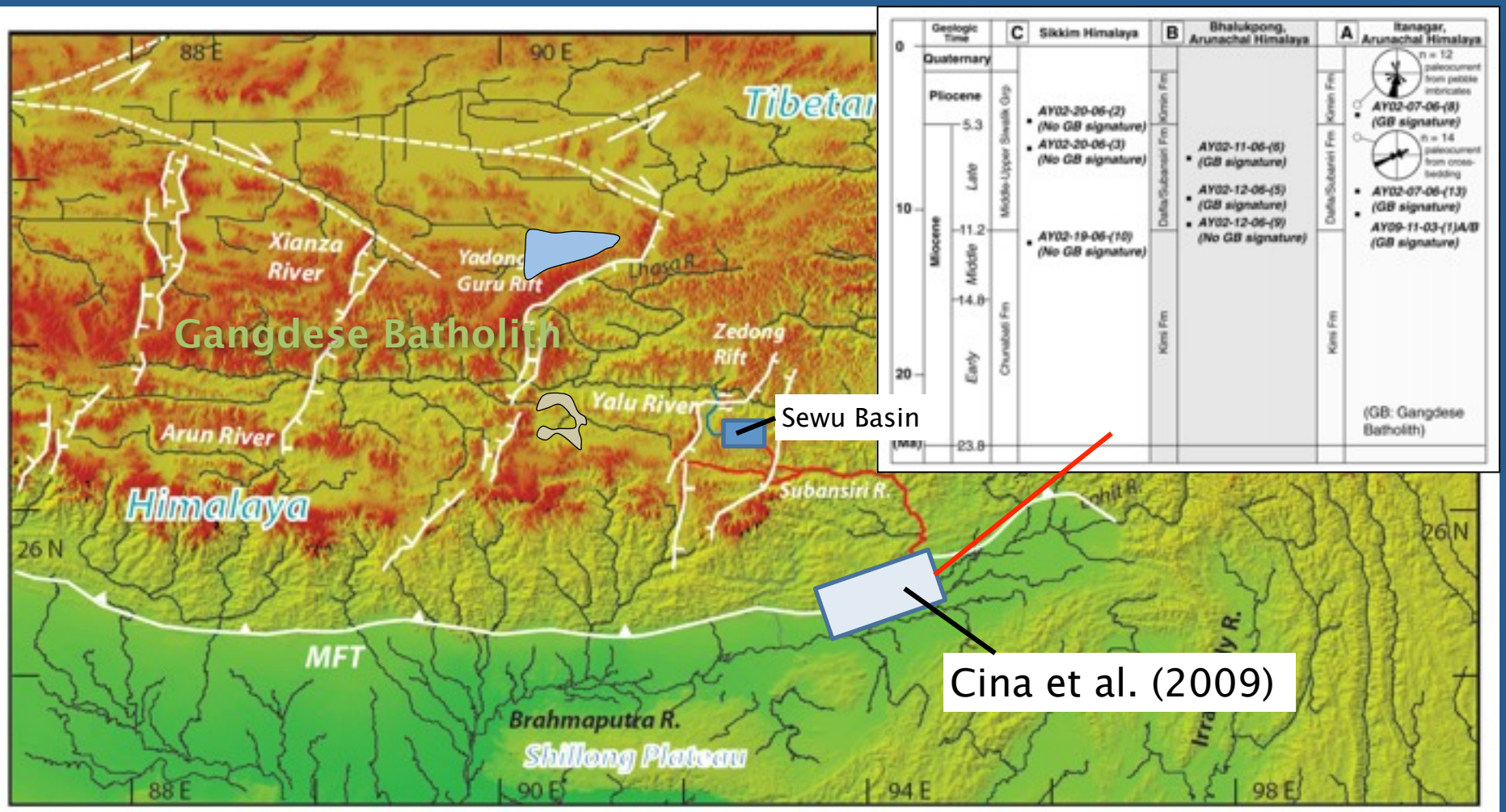

South

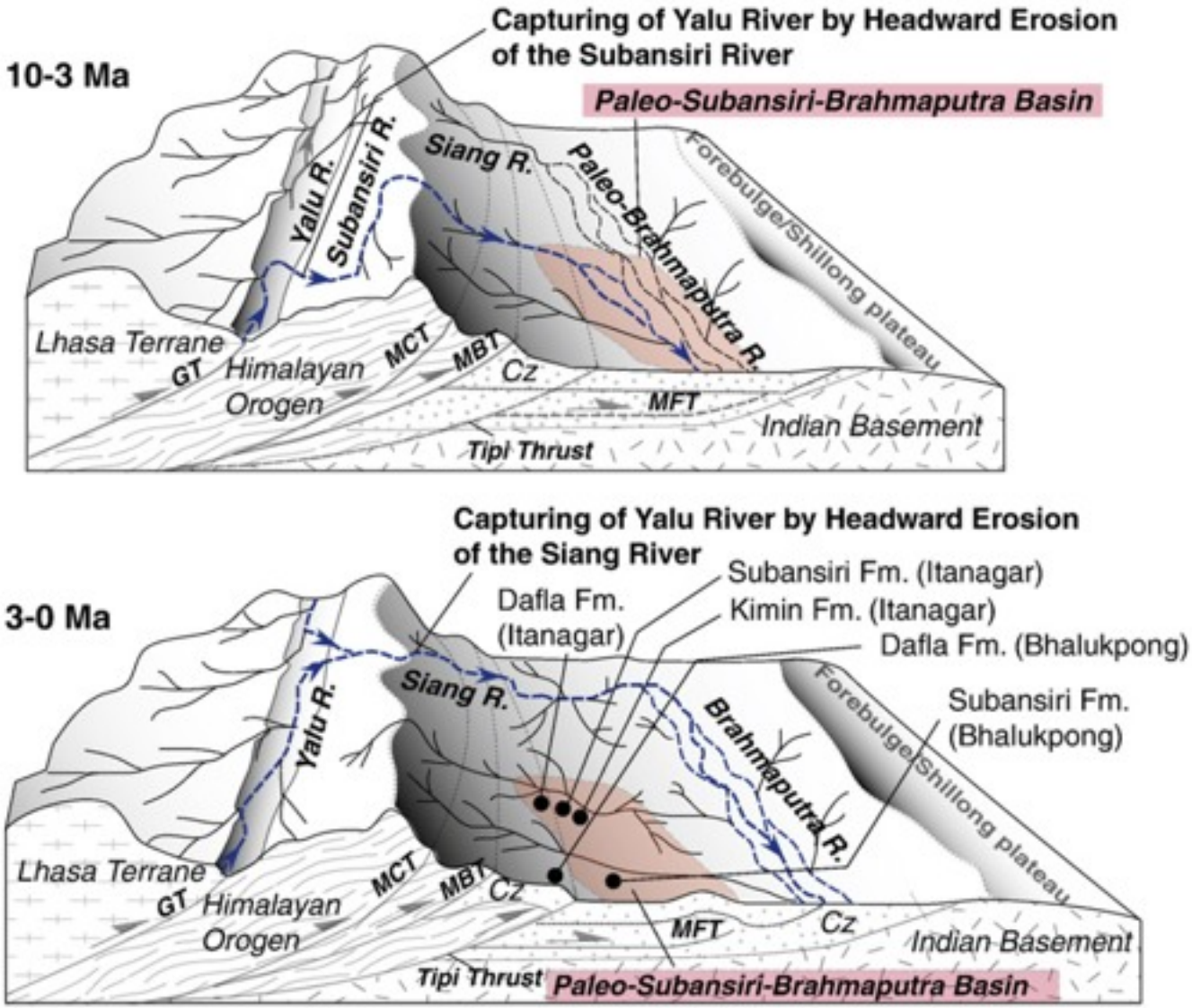
Capturing of Yalu River by Headward Erosion of the Subansiri River
10-3 Ma
Paleo-Subansiri-Brahmaputra Basin
Yalu R.
Subansiri R.
Siang R.
Paleo-Brahmaputra R.
Forebulge/Shillong plateau
Lhasa Terrane
GT
Himalayan Orogen
MCT
MBT
Cz
MFT
Indian Basement
Tipi Thrust
Capturing of Yalu River by Headward Erosion of the Siang River
3-0 Ma
Subansiri Fm. (Itanagar)
Dafla Fm. (Itanagar)
Kimin Fm. (Itanagar)
Dafla Fm. (Bhalukpong)
Subansiri Fm. (Bhalukpong)
Yalu R.
Siang R.
Brahmaputra R.
Forebulge/Shillong plateau
Lhasa Terrane
GT
Himalayan Orogen
MCT
MBT
Cz
MFT
Cz
Indian Basement
Tipi Thrust
Paleo-Subansiri-Brahmaputra Basin

Rifting caused disruption of major Himalayan drainage systems expressed by damming and ponding of large lakes

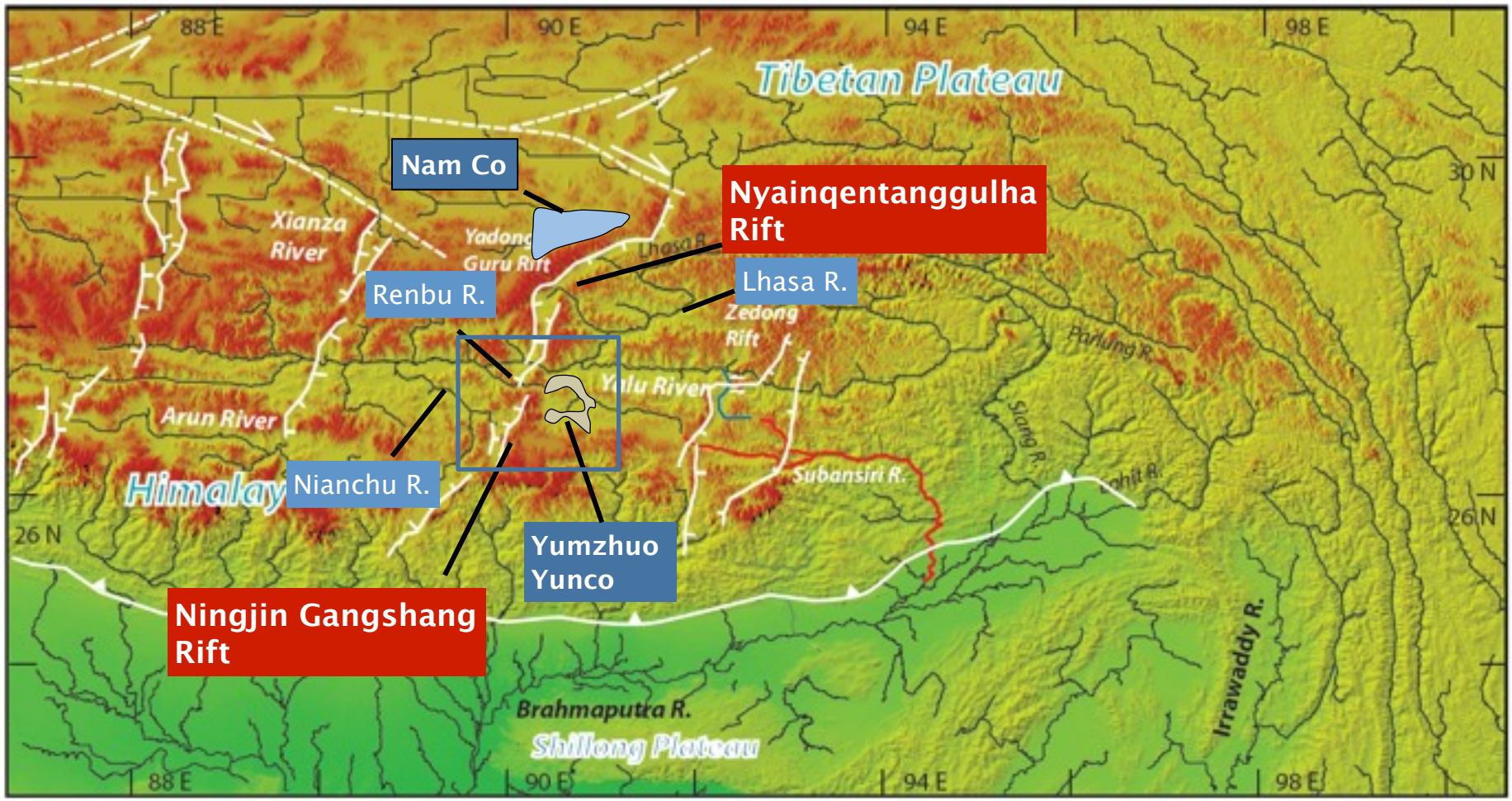

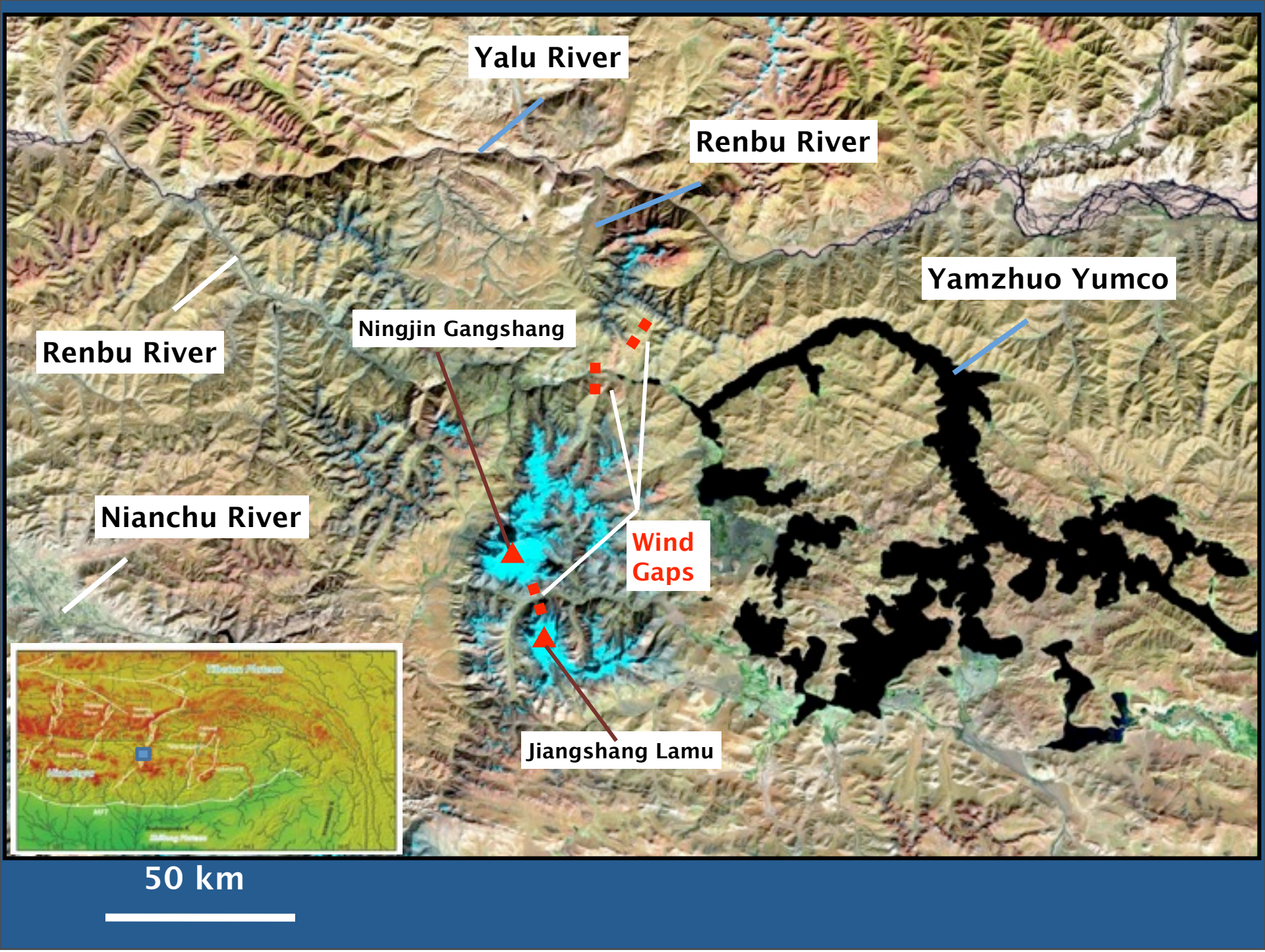

Friday, April 8, 2011

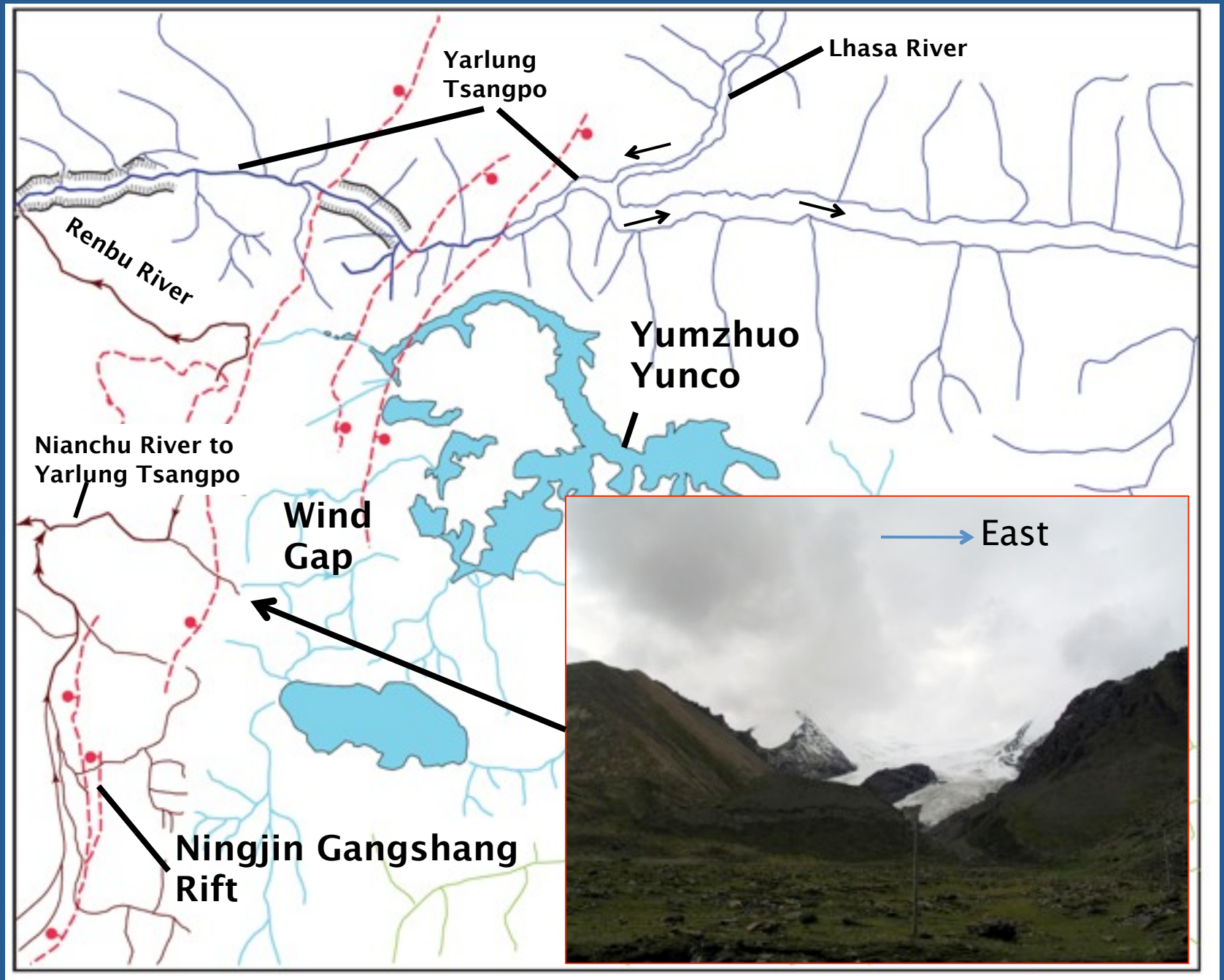
Yarlung
Tsangpo
Lhasa River
Renbu River
Yumzhuo
Yunco
Nianchu River to
Yarlung Tsangpo
Wind
Gap
East
Ningjin Gangshang
Rift

We now examine:

1. Relations between Yarlung and Subansiri Rivers.
2. Morphologic/sedimentological records for their past connection.
3. Role of climate change and tectonics in river evolution.

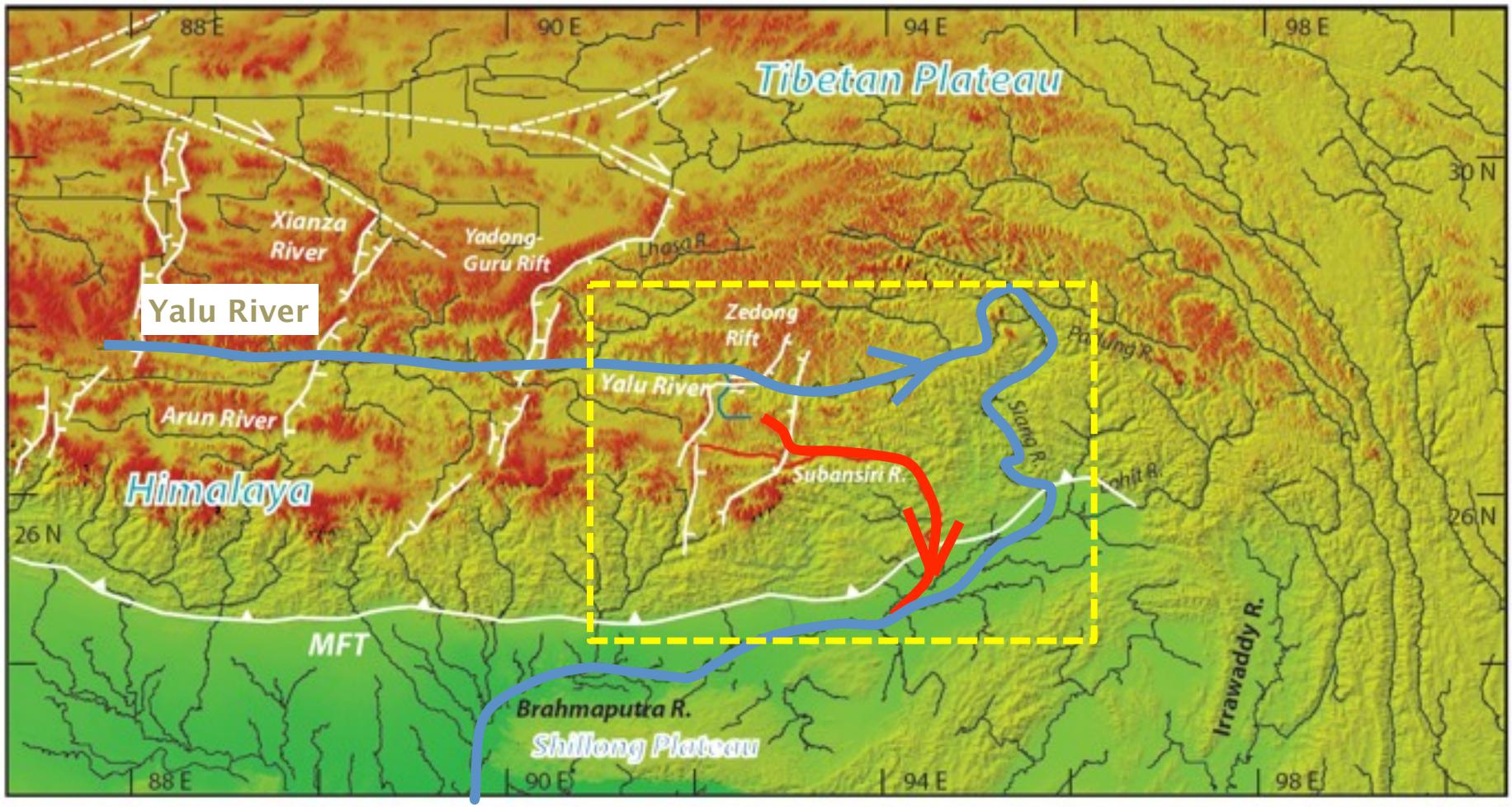

Tectono-morphologic Map of the Eastern Himalaya

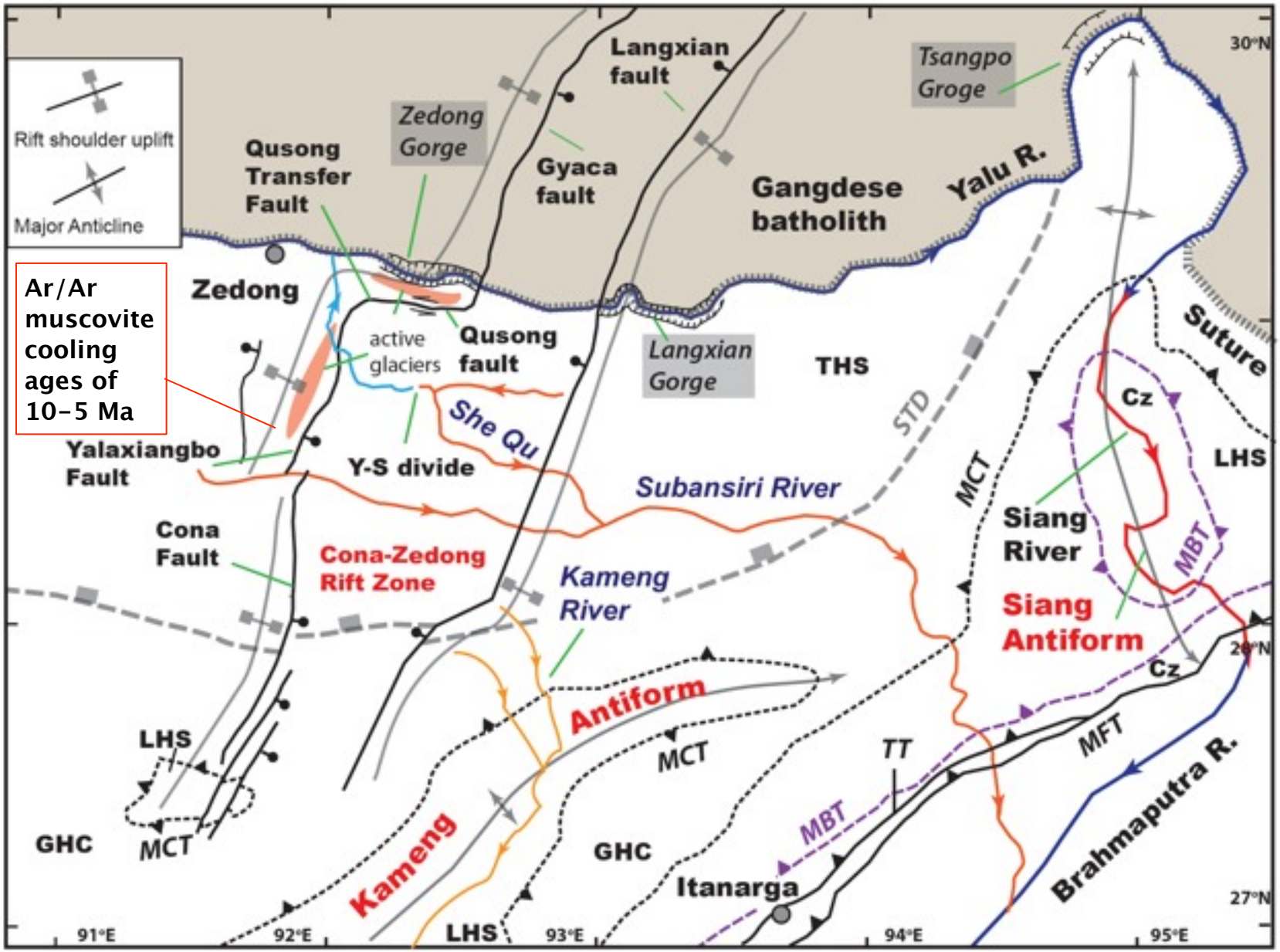

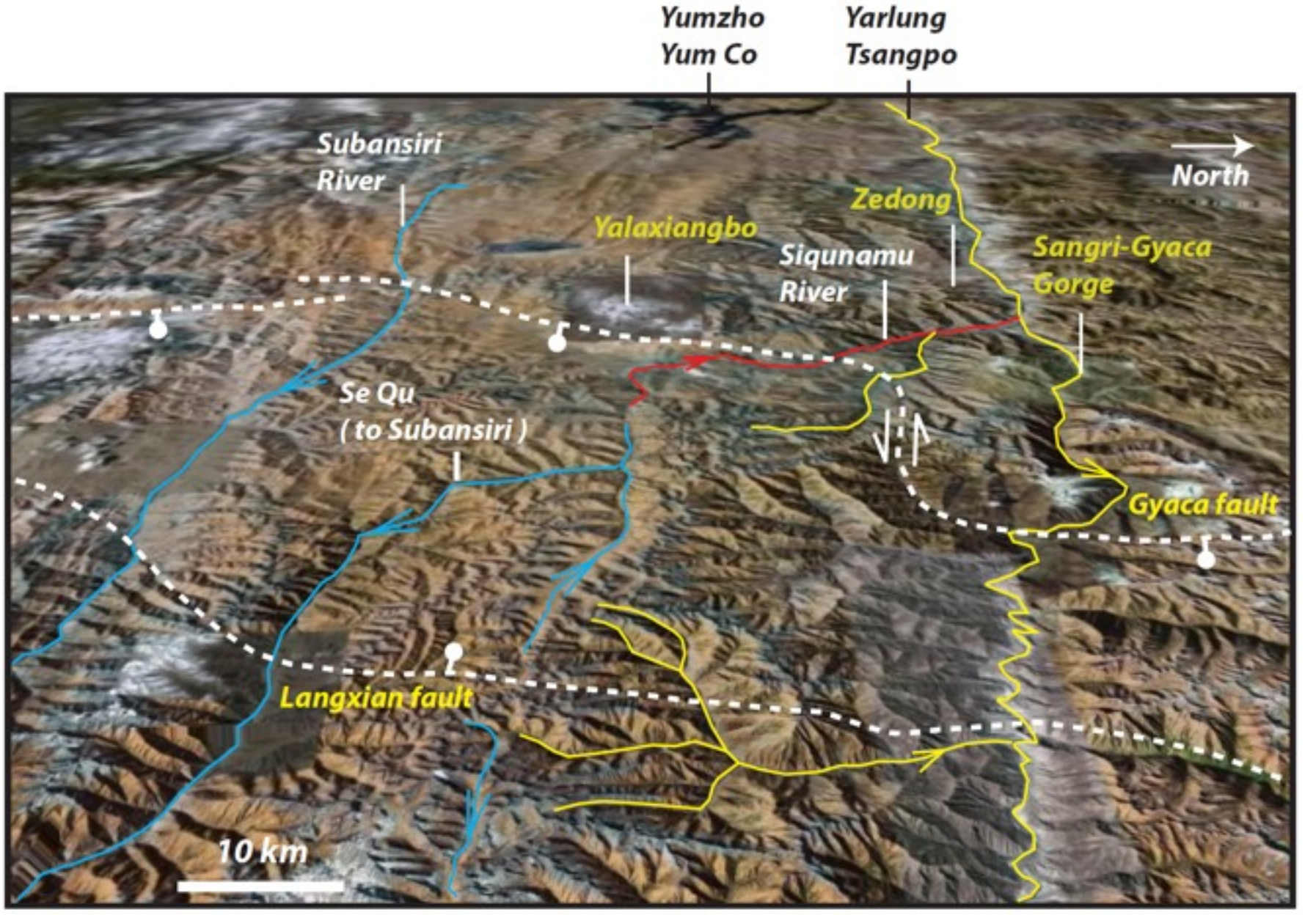
Yumzho
Yum Co
Yarlung
Tsangpo
Subansiri
River
North
Zedong
Yalaxiangbo
Siqunamu
River
Sangri-Gyaca
Gorge
Se Qu
(to Subansiri)
Gyaca fault
Langxian fault
10 km

Location of Sewu Basin

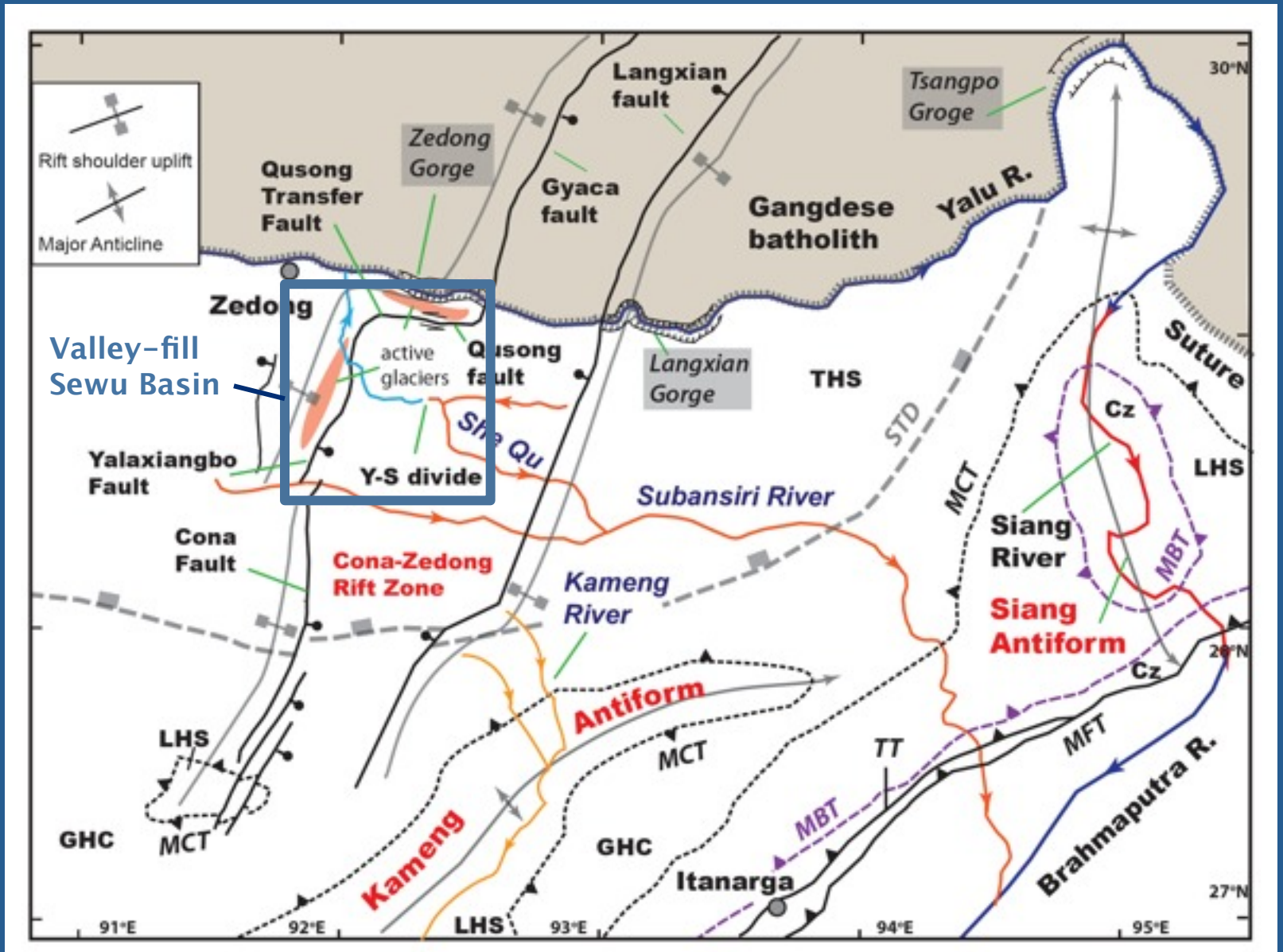

Distribution of Terraces and Channel Fill

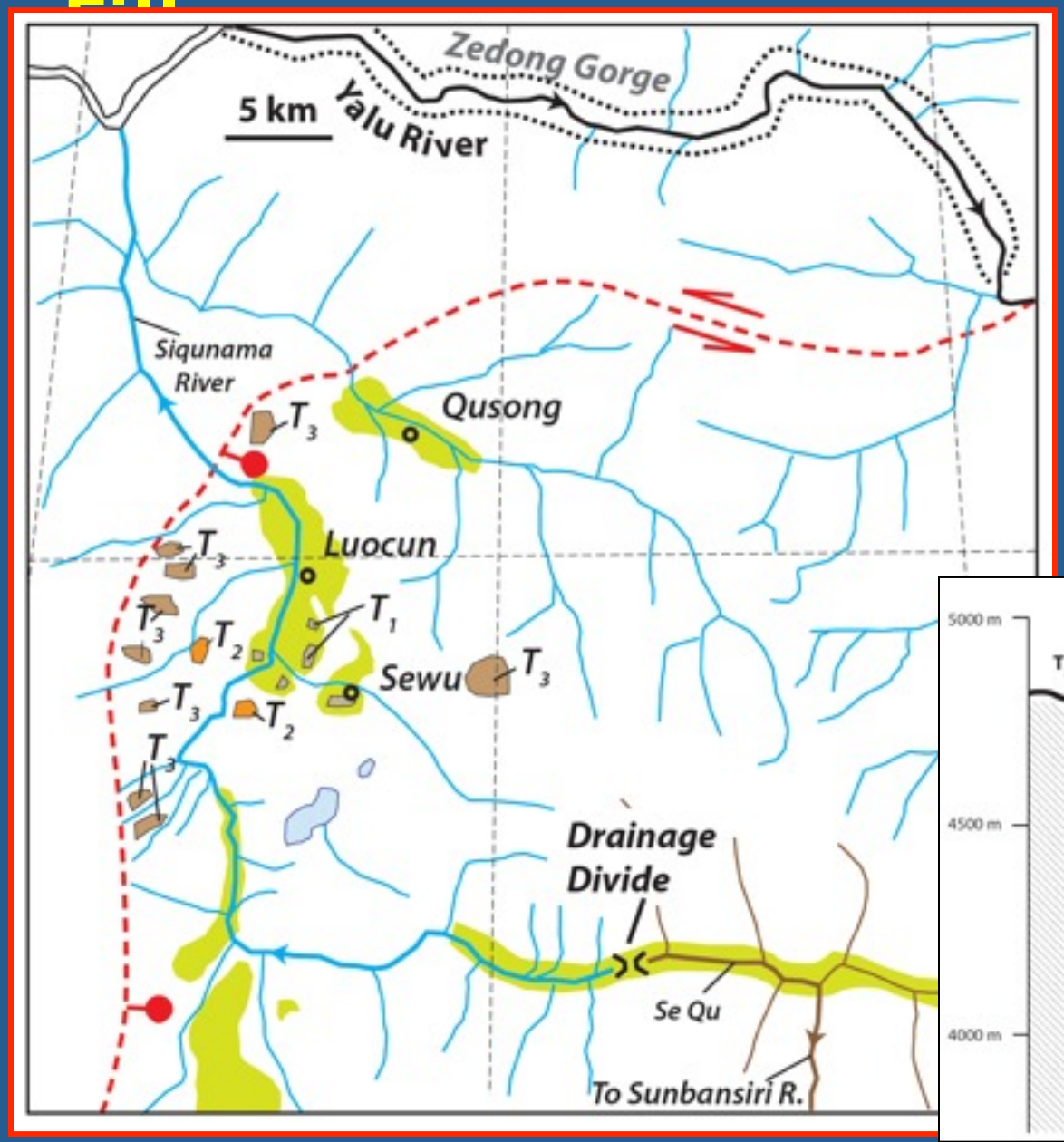

1. Channel fills can be traced from a branch of the Yarlung Tsangpo (= Siqunama River) to the Subansiri River.
2. Terrace elevations are consistent with past connection of the two rivers.

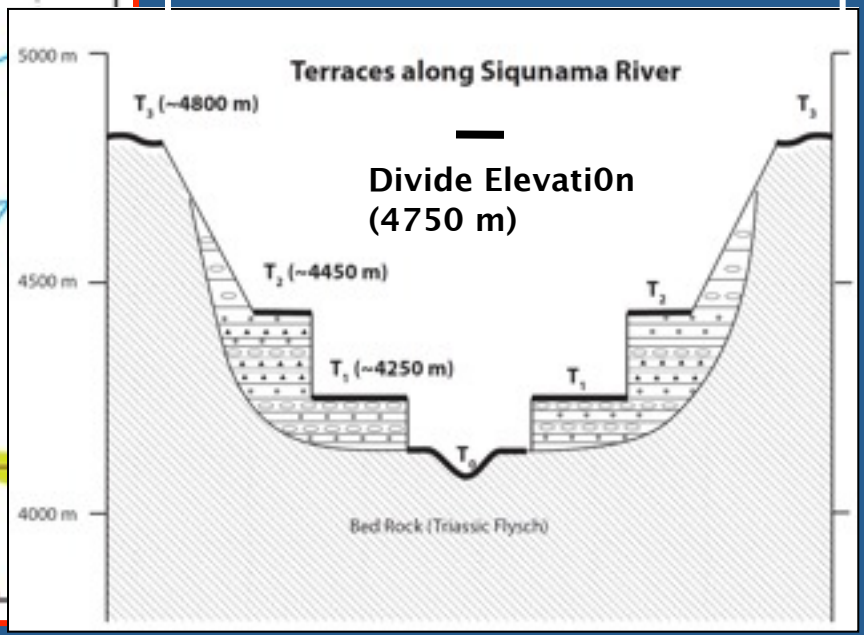

Distribution of Major Terrace Surfaces

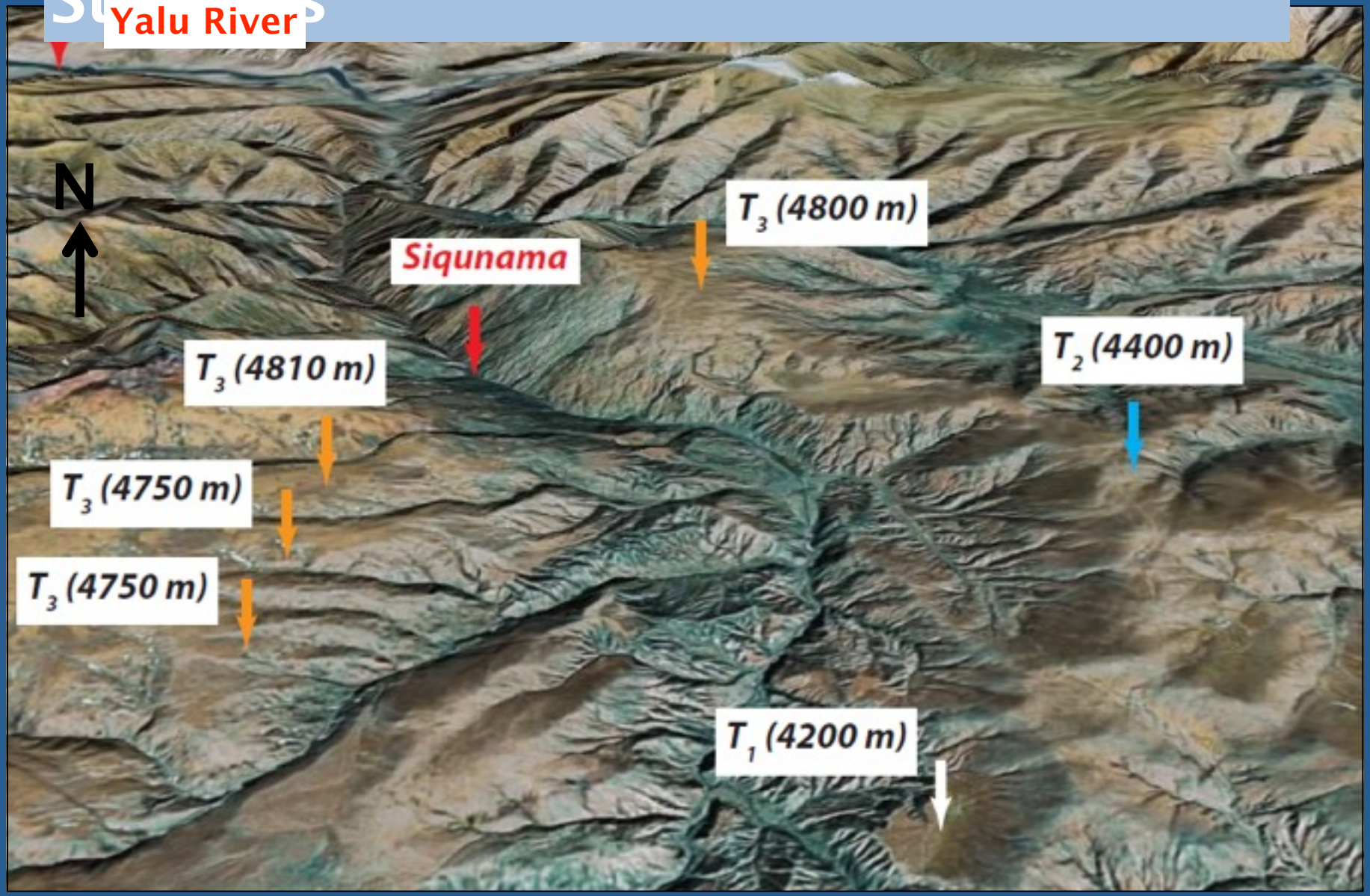

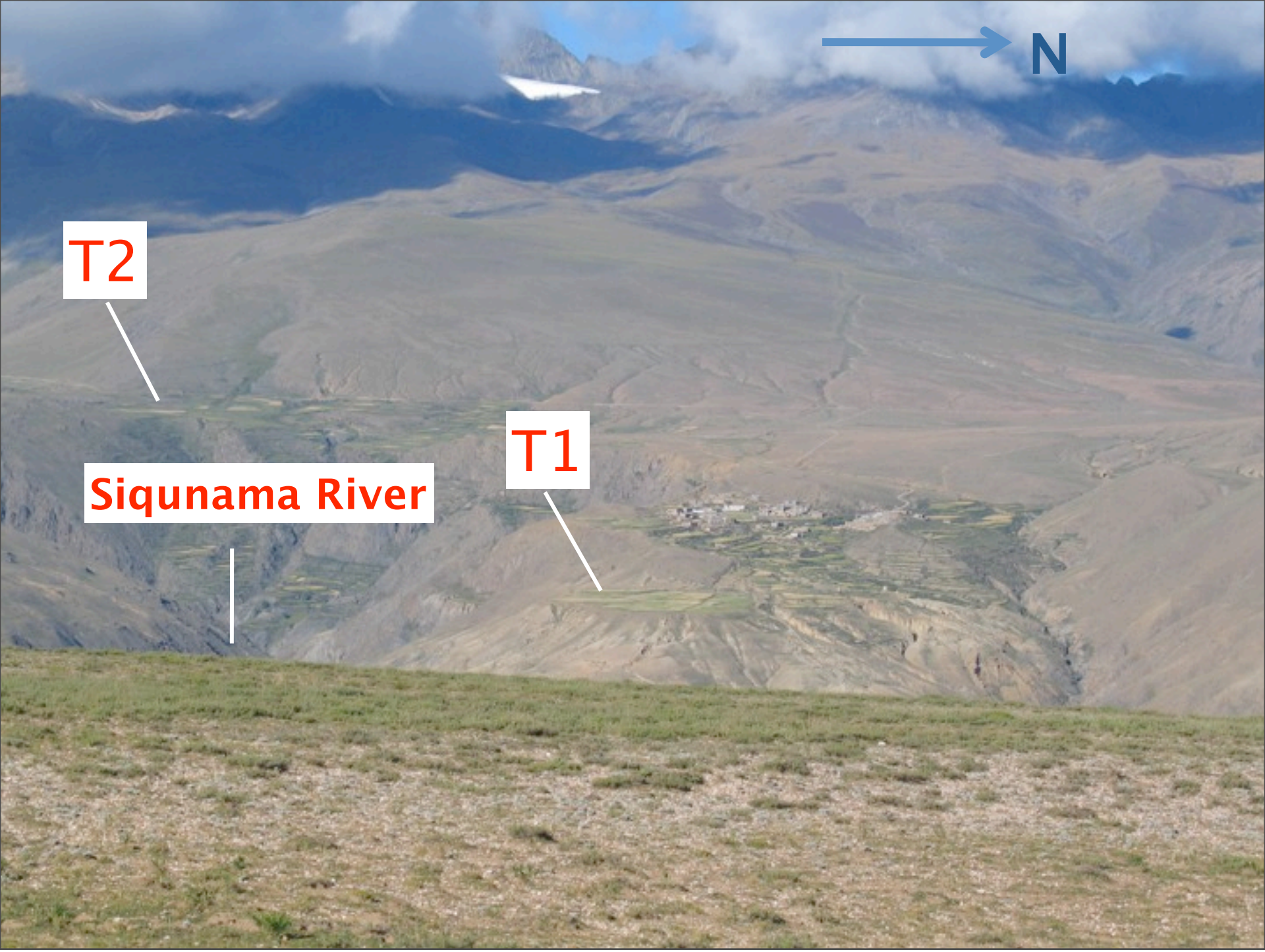
N
T2
T1
Siqunama River

Stratigraphy: Mountain-stream deposits above and below and glacial deposits in the middle section.

Paleo-current directions: Dominantly southward or eastward, opposite to current flow direction of Shiqunama River (northward and westward).

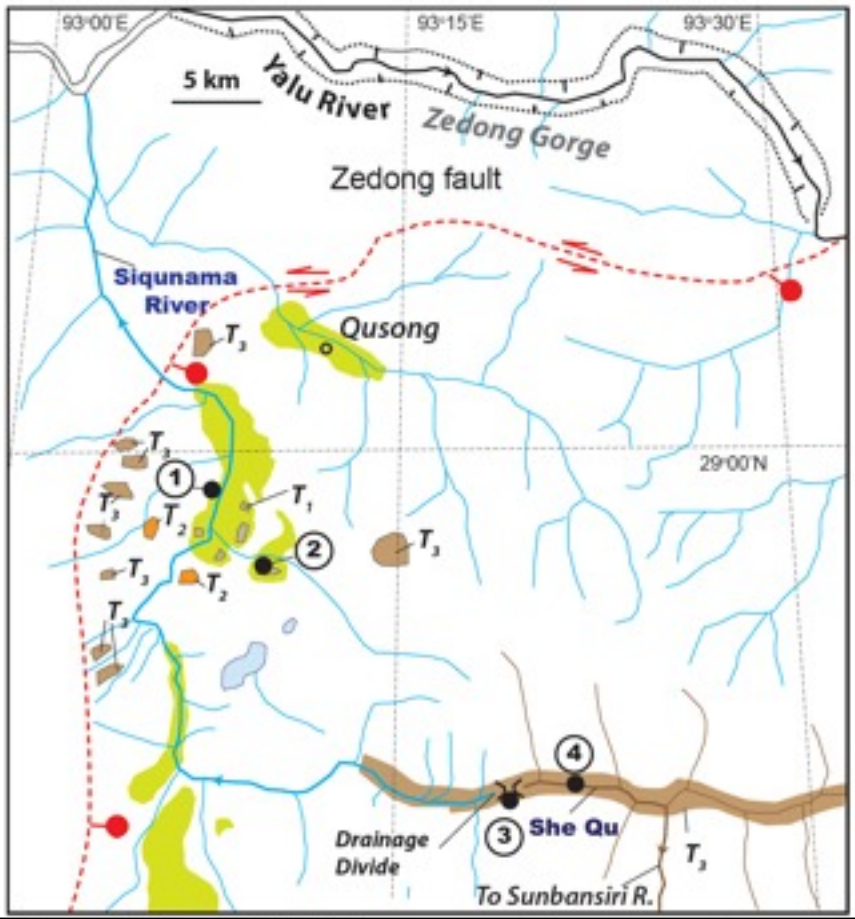

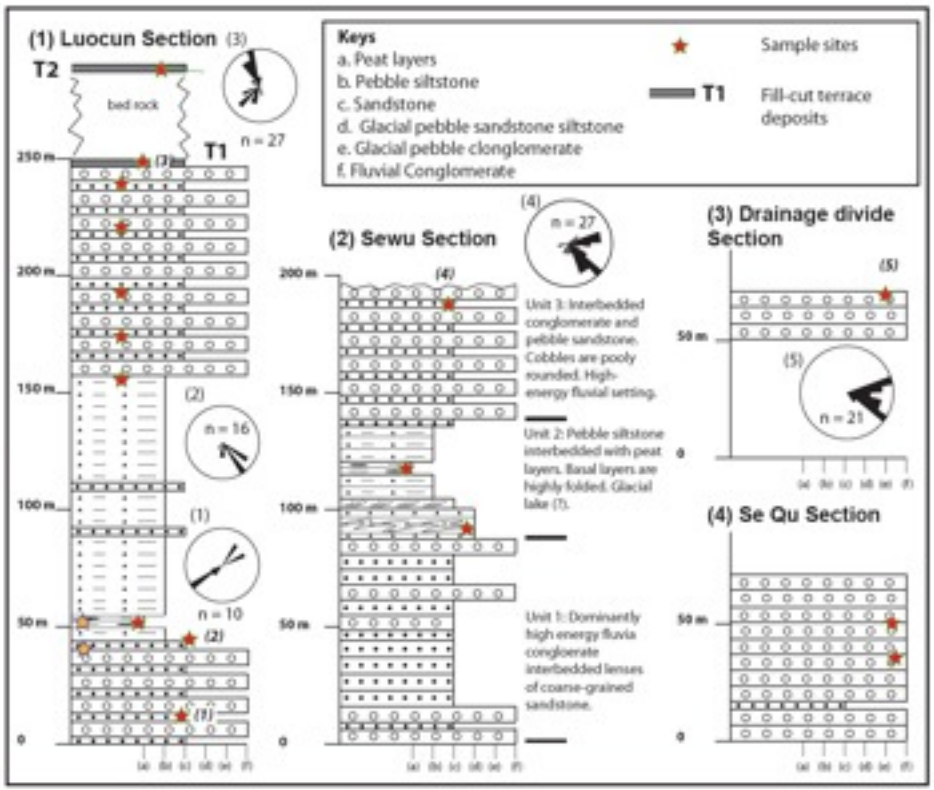

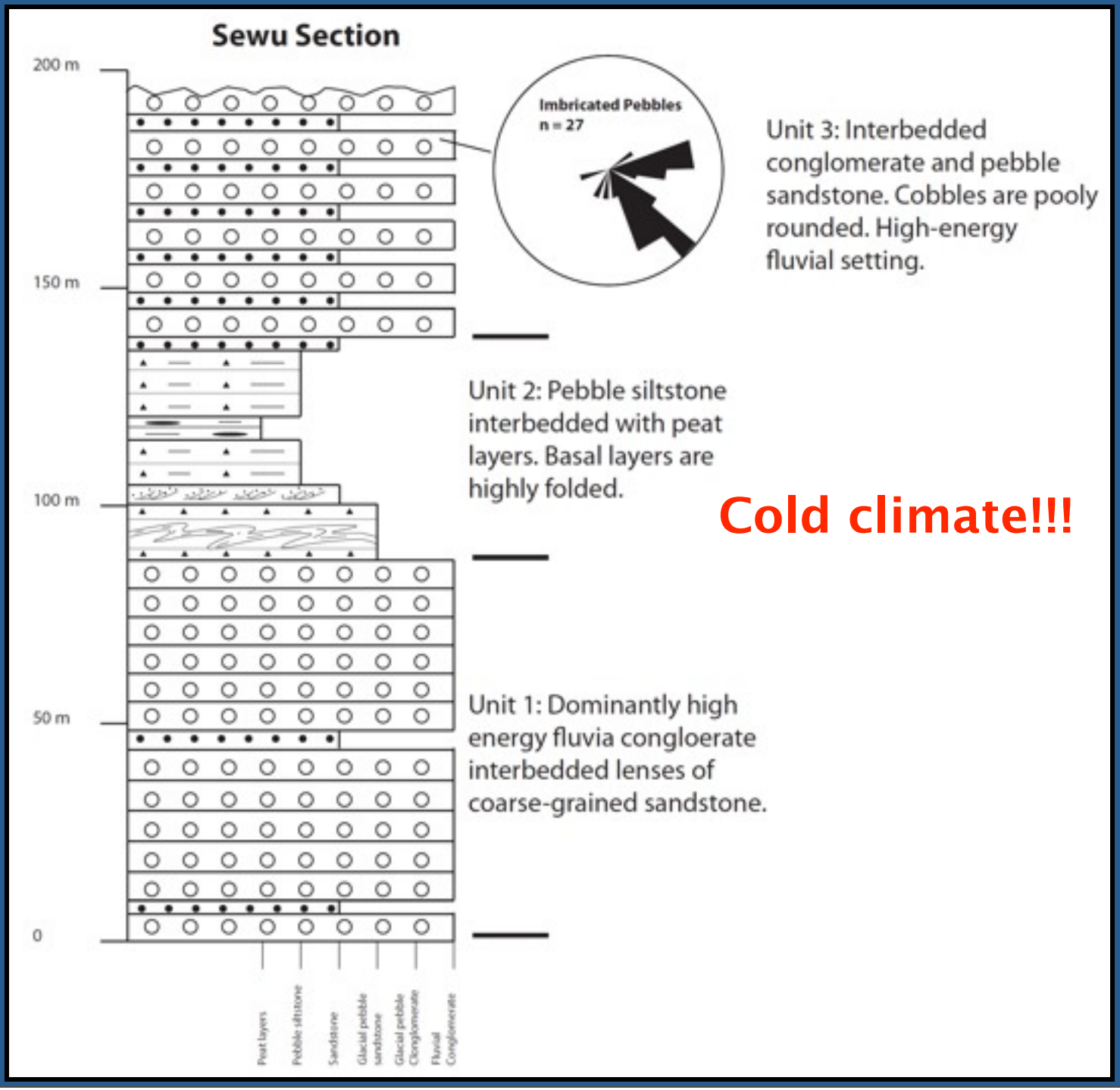
Sewu Section
200 m
150 m
100 m
50 m
0
Imbricated Pebbles
n = 27
Unit 3: Interbedded conglomerate and pebble sandstone. Cobbles are pooly rounded. High-energy fluvial setting.
Unit 2: Pebble siltstone interbedded with peat layers. Basal layers are highly folded.
Cold climate!!!
Unit 1: Dominantly high energy fluvia congloerate interbedded lenses of coarse-grained sandstone.
Peat layers
Pebble siltstone
Sandstone
Glacial pebble sandstone
Glacial pebble Conglomerate
Fluvial Conglomerate


Folded glacier deposits

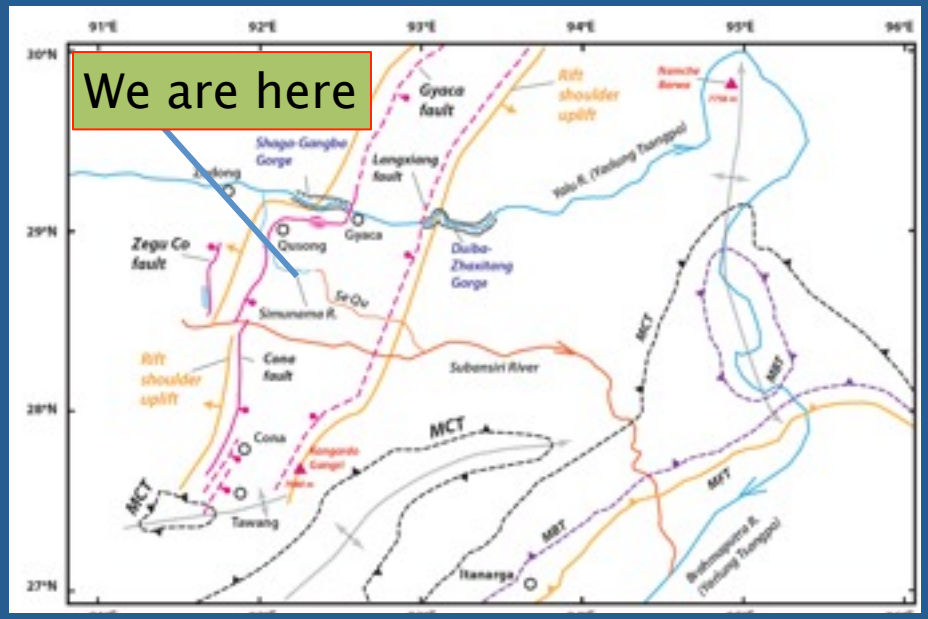
We are here
91°E
92°E
93°E
94°E
95°E
96°E
30°N
29°N
28°N
27°N
Gyaca fault
Rift shoulder uplift
Namche Barwa
Shuga-Gangbei Gorge
Lengxiang fault
Yalu R. (Yarlung Tsangpo)
Gyaca
Quxong
Zegu Co fault
Duiba-Zhaxiteng Gorge
Simunema R.
Se Qu
Rift shoulder uplift
Cona fault
Subansiri River
MCT
MBT
MFT
Cona
Kangarda Gangri
MCT
Tawang
Itanagar
Brahmaputra R. (Yarlung Tsangpo)


At divide


East
At divide

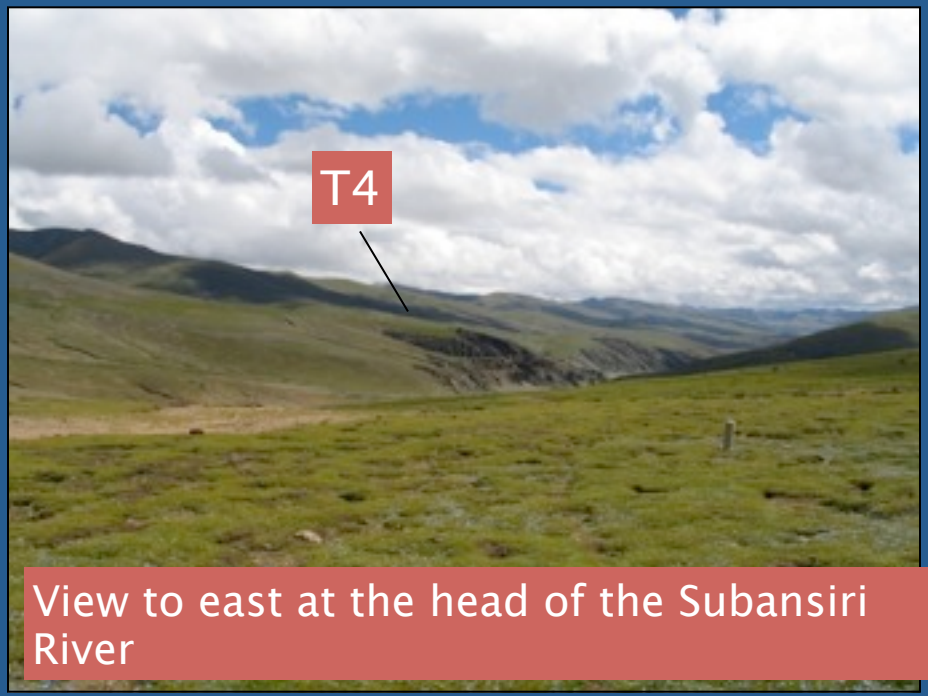
T4
View to east at the head of the Subansiri River

What caused diversion of the Yarlung Tsangpo into the Subansiri River?

We know:

(1)The diversion occurred during rifting in the past 10-5 Ma (from age of rifting controlling the Sewu basin and the age of eastern Himalayan foreland sediments containing Gangdese zircons).

(2)Valley-fill event occurred during major glacial advance (record of glacial deposits throughout Sewu basin).

Rift-induced uplift acts as a dam, which may have periodically blocked segment(s) of the Yarlung Tsangpo modulated by climate conditions.

A major glacier advance event caused shielding of the rift shoulders, allowing rift uplift to outpace downward erosion and thus forming rift dams.

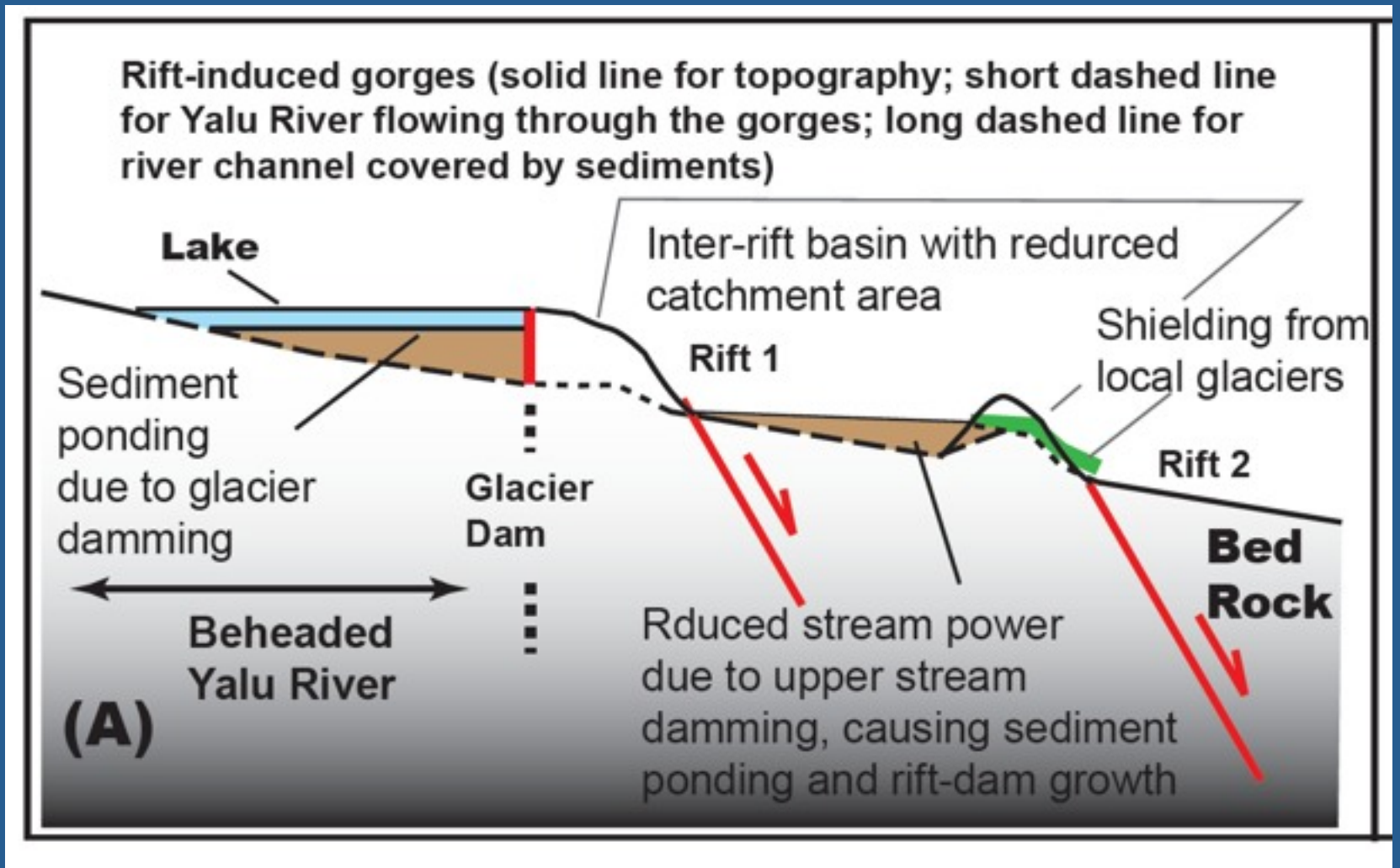

If glaciers jam the Yarlung Tsangpo river and at the same time erode the high-altitude regions of a rift shoulders rapidly, delivering the detritus to normal-fault hanging wall, then a strong feedback can lead to accelerated normal-fault slip. This process can further enhance the rift damming effect. Once this climate-induced process is removed, the river will be restored back to its original course.

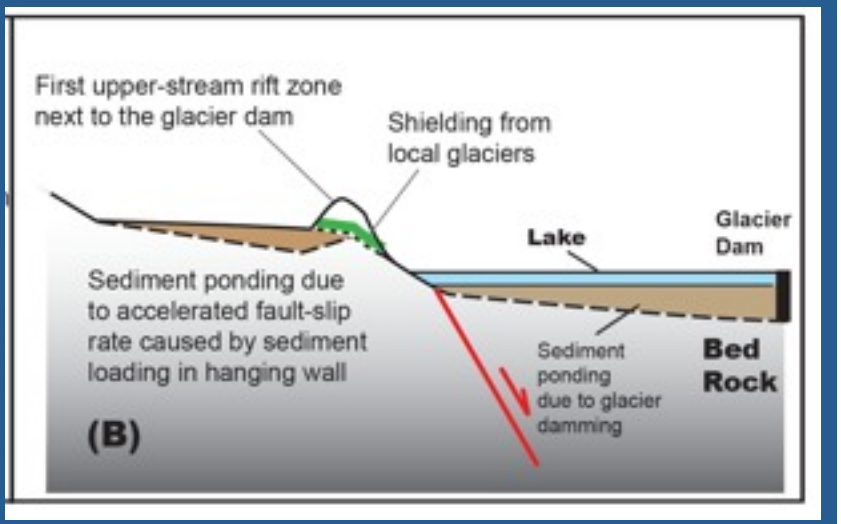

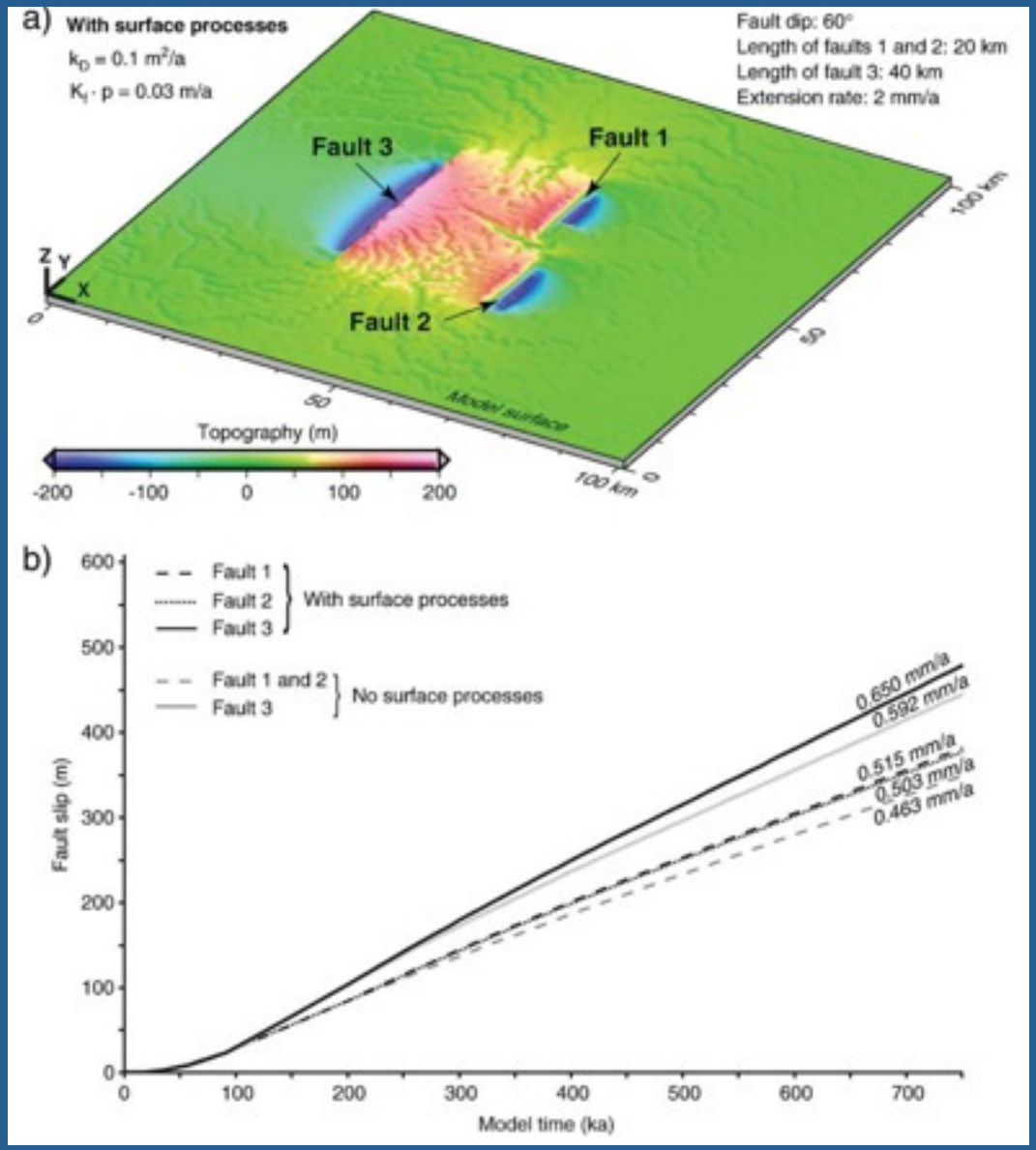

Maniatis et al. (2009, Tectonics)

(A) Major glacier advance events and slow Himalayan uplift favor rift damming and thus direct sediment transports across the range.

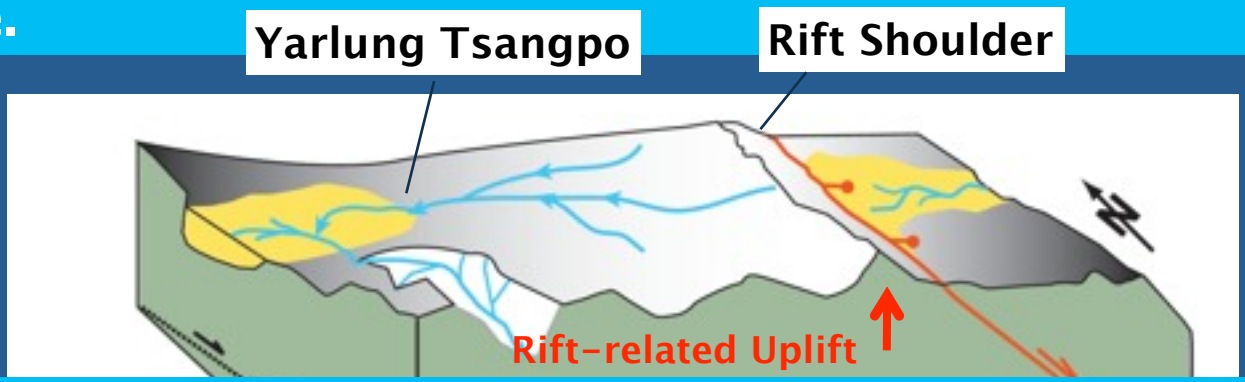

(B) Warmer climate and rapid Himalayan uplift favor east-flowing Yarlung Tsangpo and long-distance delivery of Tibetan sediments to the Himalayan foreland basin.